Effects of Macromolecular Crowding on Diffusion

A THESIS
SUBMITTED TO THE FACULTY OF
UNIVERSITY OF MINNESOTA
BY

Robb Scott Welty

IN PARTIAL FULFILLMENT OF THE REQUIREMENTS
FOR THE DEGREE OF
MASTER OF SCIENCE

Thesis Advisor: Ahmed A. Heikal

July 2013

Acknowledgements

I would like to first thank the fellow students who have helped me directly with this project: Dhanushka Wickramsinghe, Jacob Bentley, and Chang Thao.

To Dr. Erin Sheets for the use of her equipment, time, expertise, and advice. You have given me an appreciation for the wider world of biophysics, for which I will always be in your debt.

To all of the other labs in the Swenson research wing. From the professors to the undergrads I have asked you all more questions than I can remember. The kindness I have experienced within these walls has kept me going.

The Department of Chemistry and Biochemistry has shaped my understanding of science, teaching, and inquiry itself. It is the first community that I can unabashedly say that I have felt like I belonged to.

Lastly, I need to extend my gratitude to my advisor Dr. Ahmed Heikal. His influence has fostered in me a self-reliance and determination that I never thought I could have possessed.

These past few years have been among the hardest and most rewarding of my life.

Thank you

Dedication

I would like to dedicate this thesis to my father. He may take the credit for it so he can finally take his brother on their long awaited trip to Europe.

Abstract

Macromolecular crowding, the effects caused by high concentrations of macromolecules in solution, is believed to influence diffusion processes, intermolecular interactions, protein folding, and intracellular transport in living cells. The goal of this thesis was to compare translational and rotational diffusion in crowded environments to examine the effects of varying concentrations of different macromolecules on diffusion. Previous attempts have been made to characterize the effect of crowding, yet most have been unable to compare translation and rotational diffusion, and none have used model systems that offer direct comparison to other spectroscopic techniques. Using time-resolved fluorescence anisotropy and fluorescence correlation spectroscopy, we have monitored changes to the diffusion of multiple fluorescent tracers in the presences of synthetic macromolecules and proteins. These results provide new insights into the effects of crowding on multiscale diffusion, nonspecific binding, and the local heterogeneity of microviscosity experienced by different fluorophores that allow for a meaningful comparison to other spectroscopic techniques.

Table of Contents

List of Tables

List of Figures

List of Abbreviations

APD	avalanche photodiode
BSA	bovine serum albumin
CI2	chymotrypsin inhibitor 2
EGFP	enhanced Green fluorescent protein
FAn	fluorescence anisotropy
FCS	fluorescence correlation spectroscopy
FRAP	fluorescence recovery after photo-bleaching
IPTG	isopropylthio-β-galactoside
MSD	mean squared displacement
NA	numerical aperture
PBS	phosphate buffered saline
PEI	polyethyleneimine
PFG NMR	pulsed field gradient nuclear magnetic resonance
PMT	photo multiplier tube
RhG	rhodamine green
SE	Stokes-Einstein
SED	Stokes-Einstein-Debye
TCSPC	time correlated single photon counting

List of Symbols

β_i	amplitude of anisotropy decay
r	anisotropy
G	anisotropy G-factor
α	anomalous exponent
K_B	Boltzmann constant
τ_D	characteristic diffusion time
ξ	coefficient of friction
ϕ	concentration gradient
D	diffusion coefficient
x	distance
α_i	fluorescence decay amplitude
$k_{f;l}$	fluorescence decay rate
δF	fluorescence fluctuation
F	fluorescence intensity
$I_{54.7}$	fluorescence intensity at magic angle
$<\tau_{fl}>$	fluorescence lifetime
J	flux
R	hydrodynamic radius
V	hydrodynamic volume

r_0	initial anisotropy
τ	lag time
ω_z	lateral dimension of FCS observation volume
m	mass
$<x^2>$	mean squared displacement
k_{nr}	non-radiative rate constant
n	number of dimensions
N	number of molecules
$F_{\|}$	parallel polarized fluorescence
$I_{\|}$	parallel polarized fluorescence intensity
$F\perp$	perpendicular polarized fluorescence
$I\perp$	perpendicular polarized fluorescence intensity
τ_3	phosphorescence lifetime
f_3	population fraction of triplit state
ω_{xy}	radial dimension of FCS observation volume
k_r	radiative rate constant
D_r	rotational diffusion coefficient
ϕ	rotational time
c	scattering component
X	stochastic force
S	structural parameter
T	temperature

E	thermal energy
t	time
D_t	translational diffusion coefficient
η	viscosity

Chapter 1: Introduction

Starting with the pioneering work by Minton a few decades ago, macromolecular crowding has been defined as "[The] effects of excluded volume on the energetics and transport properties of macromolecules within a solution containing a high total volume fraction of macromolecules" [1]. Living cells are inherently crowded with biomolecules and organelles. Those cells may contain up to or more than 300 g/L macromolecules [2], such as proteins, nucleic acids, actin filaments, and organelles. There is strong evidence that indicates an important role of crowding on diffusion[3-6], protein folding [1, 7], and enzymatic activity [1]. To gain a full understanding of cellular processes and underlying mechanisms for cell biology, it is imperative to understand the role of macromolecular crowding in cellular processes to more completely understand cell function, survival, and diseases.

While the concept of crowding has been around since the 1940's [8], the highly cited work by Allen Minton and his coworkers reframed the topic within a biological context with an emphasis on biomolecules, namely hemoglobin [9, 10]. He postulated that when high concentrations of macromolecules were in a confined environment, the impenetrable nature of these macromolecules (also called "*excluded volume*") and their chemical structures became determining factors in the thermodynamic state of a system [9]. The advancement of modern technology has accelerated our ability to quantitatively track diffusing species, in both space and time. In a 2008 review, Verkman contrasted new fluorescence techniques to computational calculations [4]. It was demonstrated that *in*

vitro and *in vivo* studies showed crowding effects that were dependent on the sizes of macromolecules that induce crowding as well as the diffusing species. Computational modeling agreed well with the experimental results [4]. That is macromolecule-induced volume exclusion was a significant factor in describing diffusion in crowded environments.

The modeling of macromolecules as hard spheres had, up to this point, been effective at explaining deviations in classical diffusion models such as the Stokes-Einstein model. Non-steric intermolecular interactions, such as electrostatics, had either been treated as negligible or as a factor which helped determine the hydrodynamic radius of the diffusing species. The recent NMR work of Pielak has suggested that it is unrealistic to treat macromolecules as hard spheres with uniform charges [5]. He proposed that the heterogeneity of the amino acids of a given protein would lead to non-uniform surface properties which would lead to interactions with other proteins. As a result, proteins are likely to diffuse more slowly in protein-crowded environments due to the non-specific interactions among polar and charged residues. Waxham has also provided a quantitative description of the size effects of crowding agents [11]. By using many different sizes of dextran molecules as crowding agents, Waxham and coworkers have concluded that a crowding effect can be modeled as an ensemble of different microviscosities that cause solutes to diffuse at multiple discrete rates [11].

There are several studies that suggest crowding also affects biochemical reactions [7, 12]. While the underlying mechanism for a crowding effect on biochemical reactions and enzymatic kinetics is unknown, the predominant interpretation uses scaled particle theory [1, 13]. If macromolecules are treated as hard spheres, then there is an energy requirement to displace those hard spheres. For an enzyme to make a cavity in those hard spheres it must exert energy. This can result in conformational changes to reduce the volume it takes up which results in lowering the energy required to occupy that cavity. Depending on the molecular conformations of proteins, crowding could either suppress or enhance enzymatic activity. Considering that enzyme activity is dependent on conformation it makes sense, from an evolutionary perspective, that the crowded environment of cells would help select for those conformations. Also if two reactive species, such as an enzyme and a ligand, are in a crowded medium than theory suggests that if the free energy benefit is larger than the entropic penalty of the two species being held together, they will stay in close proximity to each other which would increase the chances of the enzyme and ligand interacting.

Currently, no thermodynamic model quantitatively describes the crowding effect on diffusion. Although there are some existing phenomenological and empirical models, none have been able to adequately describe the experimental data available using a wider range of experimental techniques [4]. Although some consensus has been reached on the causes and effects of crowding, the exact modeling of those remains elusive. Saxton, has written a pertinent review detailing the current gaps in our knowledge concerning

crowding [14]. Currently, for example, there is no mathematical model that describes multiscale experimental results satisfactorily. While there are many different phenomenological or empirical models that describe crowding, none have proven very effective, especially across space and time domains. Importantly, there has yet to be a model system that is amenable to a wide range of studies using myriad of spectroscopic techniques. An effective model must be applicable through different time and length scales; which will help determine the transient nature of molecular events in crowded environments.

In this thesis, translational and rotational diffusion are investigated on a wide range of time scales. More specifically, crowding effects on diffusion of multiple fluorescent tracer molecules of different sizes are examined. In these studies, biomimitic crowded environments were used as model systems which can be controlled and manipulated systematically. Complementary *in vivo* studies on crowding are beyond the scope of this thesis. In addition to rhodamine green and enhanced green fluorescent protein (EGFP) as fluorescent probes for crowding, fluorescently labeled chymotrypsin inhibitor 2 (CI2) was also used in these studies in order to allow for direct and significant comparison with NMR studies [5, 6] to elucidate crowding effects on multiscale diffusion at both the single-molecule and ensemble levels. In addition, such comparison would allow for understanding the temporal resolution and nature of readout parameters in investigating crowding. The project described in this thesis represents an important step towards gaining further insights into the effects of macromolecular crowding, both synthetic and

protein-induced, on diffusion. Our experimental findings on multiscale diffusion studies in crowded environment will help in developing a global theoretical model for describing molecular processes that occur in crowded environments.

Chapter 2: Background

2.1 How Einstein combined particle and ensemble theory

In 1855 Adolf Fick wrote the first phenomenological law for diffusion, his model was adapted from the heat conduction equation by Fourier. In Fick's first law, the diffusive properties of salts dispersing in water is in terms of the dependence of flux (J) on concentration (φ) [15] and a diffusion coefficient (D) such that [16].

Equation 2.1

$$J = -D\frac{d\varphi}{\mathrm{dx}}$$

The time-dependence of solute concentration, the rate of change of concentration per unit time, also known as Fick's second law, depends on both the diffusion coefficient and the second derivative of concentration such that:

Equation 2.2

$$\frac{d\varphi}{\mathrm{dt}} = -D\frac{\delta^2\varphi}{\delta x^2}$$

Fick's laws are unable to relate macroscopic diffusion to the movement of single particles.

In 1828, Brown investigated the random motion of pollen grains diffusing in water, which was later termed "random walk" and more recently as "Brownian motion". The problem encountered by investigators in trying to characterize the movement of single particles is that they do not possess a constant velocity. In 1905 Einstein realized that

instead of trying to relate the movements of diffusing particles to their velocity it was imperative to relate their movement to distance traveled [15]. Considering the stochastic nature of the diffusion process, Einstein reasoned that the average distance traveled by a particle undergoing Brownian motion was nil. However, the mean squared displacement (MSD) provides an alternative physical quantity for determining the total distance traveled in n dimensions during a time period (t) such that:

Equation 2.3

$$\langle x^2 \rangle = 2nDt$$

This equation is also known as Einstein-Smoluchowski relation. The validity of this relationship was established by Perrin [17]. Perrin suspended micro-particles in solution and then tracked their movements via microscope. By recording their position at regular intervals, he was able to determine their MSD (or $<x^2>$).

Einstein also concluded that the rate of diffusion was determined by the interplay between thermal energy that caused the movement of a particle and the corresponding friction (ξ) between the particle and its surroundings environment. Which is referred to as the Stokes-Einstein equation (equation 2.7) [15, 18]:

Equation 2.4

$$D = \frac{E}{\xi}$$

The thermal energy of a particle was defined as.

Equation 2.5

$$E = k_B T$$

The friction coefficient was taken from the work of Stokes, some fifty years earlier, by the size of the diffusing species, its shape, as well as the viscosity of surrounding environment. For example, the friction experienced by a spherical particle of a low Reynolds number is given by Stoke's law [19]:

Equation 2.6

$$\xi = 6\pi\eta R$$

Equation 2.7

$$D_t = \frac{K_B T}{6\pi\eta R}$$

Rotational diffusion can also be defined similarly, though the friction coefficient is adjusted to account for the whole surface area being subject to friction, by the Stokes-Einstein-Debye equation [20].

Equation 2.8

$$D_r = \frac{K_B T}{8\pi\eta R^3}$$

The Stokes-Einstein and Stokes-Einstein-Debye equations have accurately described the motion of diffusing molecules under many conditions, but its accuracy is currently being questioned in complex solutions[21]. My experimental work, presented in later chapters, will explore the validity of the Stokes-Einstein and Stokes-Einstein-Debye equations by

comparing the effect of viscosity on the diffusion coefficient in complex, and biologically relevant, solutions.

One reason why the Stokes-Einstein and Stokes-Einstein-Debye equations may not adequately describe diffusion is based in the assumption that solutions will act as a continuum. By looking at diffusion from the perspective of individual particles it is possible to model more complex solutions. In 1908, Langevin related Einstein and Smoluchowski's understanding of diffusion to the velocities of individual particles. He reasoned that the force acting on any individual particle was determined by its current velocity and the sum of the collision forces acting on it such that [22]:.

Equation 2.9

$$m\frac{\delta^2 x}{\delta t^2} = -\xi\frac{\mathrm{dx}}{\mathrm{dt}} + \xi X$$

Where the stochastic force, X, is a result of collisions of the diffusing species with surrounding molecules caused by the thermal energy of the system. While this model is not used in the analysis of my experiments, it is useful to keep in mind while discussing diffusion. By thinking of diffusion in terms of individual collision we can gain an appreciation for not only differences in collisions between different types of molecules but the time scale that they take place on.

2.2 Volume exclusion and anomalous diffusion

The previous section describes mathematical treatments for a diffusing particle undergoing Brownian motion. Under certain environmental conditions, however, diffusion of a given species may deviate from Brownian motion, which is called

"anomalous diffusion" [23]. Anomalous diffusion is thought to arise in complex systems, where physical obstructions either permeate or make up the system such as mesoporous matrices, nanofabricated lattices, crowded polymer solutions, and lipid membranes [14, 24-26]. For example, anomalous diffusion has been detected in synthetic zeolites, a mesoporous aluminosilicate, with small organic molecules (e.g. methanol) detected with pulsed field gradient NMR [24]. Here, however, I will confine my discussion of anomalous diffusion that originate exclusively from biological or biomimetic crowding.

In Brownian diffusion, the stochastic force obeys the central limit theorem as described above (equation 2.9). In the case of anomalous diffusion, however, this does not occur and the mean squared displacement has a non-linear time dependence such that [14]:

Equation 2.10

$$\langle x^2 \rangle = 6Dt^{\alpha}$$

The anomalous exponent α signifies the degree of deviation from Brownian diffusion (where $\alpha = 1$). The mechanism(s) behind the non-linear time dependence is still unknown, but there are many different possible causes discussed in literature such as: hard interactions between diffusing particles (volume exclusion) [9], soft interactions (non-specific binding)[6], and differences in short/long time dynamics[27]. For any of these, or any other, causes to result in anomalous diffusion, the stochastic force exhibited on a diffusing particle (equation 2.9) is non-Gaussian, and/or (an) additional force(s) must be acting on the diffusing particle. Mathematical models which address this both

phenomenologically and mechanistically [28] are reviewed by Bouchaud and Georges [8] as well as Metzler and Klafter [29].

Volume exclusion has been attributed to causing anomalous diffusion and to affecting how viscosity is perceived by different molecules. The anomalous diffusion argument is that the crowding agents in crowded solutions physically obstruct the movement of diffusing molecules causing their MSD to have a non-linear relation with time (as in equation 2.10). To verify whether anomalous diffusion is dependent on volume exclusion groups have used FCS to quantify α (using equation 3.5). The results of those experiments are in good agreement with computer simulations of theoretical models of crowding dependent anomalous diffusion [30-32]. Whether or not the experimental values were correct is a matter of disagreement, with some groups being unable to reproduce the same results [4]. Others proposed that the perceived anomalous diffusion was actually an artifact caused by tracers moving at multiple rates [11].

Volume exclusion is also thought to possibly change rates of diffusion as a function of crowding agent characteristics (such as size and shape) and concentration while still exhibiting Brownian motion [9]. In 1951 Mooney suggested that the Stokes-Einstein equation was only valid only at infinite dilution [33], (i.e. where the diffusing species only interacts with solvent). He suggested that the bulk viscosity of a solution was not always the same as the viscosity sensed by diffusing molecule. This means that crowded solutions would exhibit different viscosities depending on the nature of the crowding

agent and diffusing species. He defined viscosity as a function of the size of a crowding agent, its concentration, and a substance specific constant. Since then multiple studies have come out supporting this idea of microviscosities that differ from macroviscosity [9, 34, 35]. To further complicate the matter, recent work has suggested that crowding may cause solutions to exhibit multiple detectable microviscosities [11].

2.3 Soft interactions

Above, diffusion has been discussed in terms of hard interactions caused by steric repulsions. In contrast, soft interactions are non-covalent chemical interactions among solutes and crowding agents [6]. As a result, soft interactions are sensitive to the chemical structure of solutes and crowding agents, which may lead to varying degrees of non-specific binding. To understand the effect of crowding in a biological context it is important to consider biological macromolecules, such as proteins, have complex surfaces that consist of polar, non-polar, and charged amino acid residues. The structures of chaperones, for example, are directly linked to their non-specific interactions with target proteins which activate their biological function [36, 37]. When compared to synthetic polymers, however, proteins have been shown to exhibit different effects on protein diffusion [5, 6, 34]. This suggests that in some biologically relevant cases soft interactions can have quantifiable effect on diffusion.

2.4 Limitations of current methods

Elucidating the effects of macromolecular crowding on diffusion and the underlying mechanism (e.g., anomalous diffusion) has been hindered by the limitations of modern

techniques [14] such as the lack of an experimental control usable over multiple distance and time scales. For example, NMR has been used to investigate macromolecular crowding on the diffusion of CI2 [5, 6, 34]. However, NMR is inherently limited to specific time scales (milliseconds to seconds), displacement distances (10-100 nm) [38], and are only capable of looking at ensembles of diffusing species. Fluorescence recovery after photo-bleaching (FRAP) is also limited to ensemble studies in addition to the resolution of the camera. Fluorescence correlation spectroscopy, FCS, has single molecule sensitivity which is superior to NMR, detects a much small volume than FRAP, and has microsecond resolution. However, unlike FRAP, FCS is restricted to a single time scale, and low tracer concentration. In a 2008 review Verkman has also cast doubt on the reliability of FCS in cells, which can be "confounded by reversible photophysical processes, cell autofluorescence, and complexities in beam and cell geometry" [4].

Determining rotational diffusion presents other difficulties, most prominently a lack of techniques to observe rotational diffusion. Considering NMR works in the millisecond to second time scale and fluorescence anisotropy can only detect rotation in the timescale of fluorescence lifetime (typically picosecond to nanosecond) [39], there is little, if any, mention of detecting rotational diffusion in an intermediate time scale in available literature. This clearly demonstrates the need to compare the results of different techniques.

Chapter 3: Materials and Methods

3.1 Rationale for sample choices

To test for the effects of crowding on diffusion, a controlled environment with variable concentrations of crowding agents is needed. The criteria for choosing the crowding agents used in these studies are solubility, surface structure, size, and availability. It is also important to use macromolecular concentrations that mimic cellular environment, which is estimated to be ~300 g/L [2] as determined using refractive index measurements [40]. In addition, the globular crowding agents were chosen to be relatively larger in size than the tracer fluorophores. Crowding agents that had been used by other groups would also allow for relevant comparison with literature studies for cross referencing that is important for model building. Fluorescent probes were chosen on the basis of photostability, availability, size, and their use in other crowding experiments.

3.2 Buffers and viscous continuum as a control

Phosphate buffered saline (PBS) buffer was used for all of the crowding agents. To discriminate between the viscosity and crowding effects on diffusion, buffers with variable concentration of glycerol (93 Da) was used to create a viscosity-specific continuum. Glycerol was purchased from Alfa Aesar (99.5+%, CAS # 56-81-5). The fluorescent probes (rhodamine green and EGFP) were added just before the experiments at 10 nM and 2 μM concentrations for FCS and time-resolved anisotropy experiments, respectively.

3.3 Crowding agents and sample preparations

Both synthetic molecules and proteins were used as crowding agents in these studies. For synthetic crowding agents, Ficoll 70 (70 kDa) and Ficoll 400 (400 kDa) were purchased from Sigma Aldrich and GE Healthcare (CAS # 17-0310-10 and 17-0300-10 respectively) and were used in these studies without further purification. Ficoll is a synthetic polymer made from cross-linking sucrose monomers [41] and has been used previously in crowding experiments [6] due to its high solubility as well as its globular form. The globular nature of Ficoll has been under some scrutiny recently [41] due to its potential tendency to deviate from a globular shape at higher concentrations (> 100 g/L) where they may form a meshwork [34, 42].

For proteins as crowding agents, we used bovine serum albumin **(**BSA) and ovalbumin from chicken egg white. BSA is a serum transport protein [43]; ovalbumin has an unknown function and is found in large quantities in avian egg white [44]. BSA and ovalbumin were purchased from Sigma Aldrich and were used without further purification. Both are globular proteins with isoelectric points of 4.7 and 4.6; and molecular weights of 66 kDa and 45 kDa respectively (CAS 9048-46-8 and 9006-59-1, respectively.) The viscosities of Ficoll and glycerol at 20°C were determined with Ubbelohde viscometers (Cannon Instrument Co.). The viscosities of BSA and ovalbumin solutions were taken from [6].

3.4 Solute molecules (fluorescent probes)

Rhodamine green, RhG, (507.9 Da) is a photo-stable dye (Invitrogen.) In addition to its use as a probe for crowded environments, RhG was also used as a control to determine FCS detection volume and to calibrate the time-resolved anisotropy setup. For FCS experiments 1–6 nM concentrations of RhG was used as compared with 1–6 μM concentrations for TCSPC techniques. The absorption and emission spectra peaks are around 504 nm and 532 nm, respectively.

Enhanced green fluorescent protein, EGFP, is a recombinant protein mutated from a gene isolated from the jellyfish *Aequorea victoria* [45]. EGFP was purchased from BioVision and was used without further purification. The excitation and emission of EGFP in a buffer peaks at 488 nm and 507 nm, respectively. It was used at concentrations of 1–10 nM for FCS and 1–10 μM with Time correlated single photon counting, TCSPC, techniques.

Fluorescently labeled chymotrypsin inhibitor 2 (CI2) was another probe for crowding. A DNA plasmid containing a gene for CI2 with I37C mutation and kanamycin resistance was a gift from Dr. Gary Pielak (the University of North Carolina at Chapel Hill). The plasmid was transfected via heat shock into BL-21(DE gold) star strain of *Escherichia coli* (Invitrogen). A single colony of the transfected *E. coli* was cultured and stored in a glycerol solution in a -80 °C freezer for further use as needed. A starter culture of 100 ml of LB broth was inoculated with the glycerol stock and incubated in the afternoon. The next morning an absorbance measurement was taken and the culture was added to

900 ml of LB broth and further incubated. When the primary culture had the same absorbance as the starter culture (i.e., arrival in late log phase) the culture was induced with isopropylthio-β-galactoside, IPTG. Five hours after being induced, the culture was taken out of the incubator and was centrifuged for 20 minutes prior to being sonicated on ice for 10 minutes (10s on 10s off at 50% power.) The lysate was centrifuged for 20 minutes 3 times. Polyethyleneimine, PEI, was added to the supernatant for a final concentration of 0.2% and then stirred on ice for 30 minutes. The supernatant was then centrifuged at 21,000xg for 20 minutes twice. The lysate was then filtered through a 0.2 μm. The lysate was then run through a Q sepherose column (GE Lifesciences), which has been equilibrated with 25 mM Tris-HCL buffer (pH8). CI2 was located in the run through and was collected and then concentrated with a 3,000 MW cut off Amicon Ultra-15 Centrifugal Filter Unit (Millipore). Purity was assessed by an 18% SDS-PAGE with a Coomassie blue stain..

CI2 was labeled with alexa-flour-488 C_5 malimide (Invitrogen). Alexaflour was diluted in DMSO. The tris-HCl buffer that CI2 was in was replaced via the amnicon with 20mM phosphate buffer with pH 7. CI2 (2 mg) was mixed with alexa-flour at 2:1 molar ratio in the phosphate buffer for 4 hours at room temperature followed by the removal of any excess AlexaFlour using an amicon.

3.5 Fluorescence correlation spectroscopy (FCS)

3.5.1 Theoretical background

FCS is a single-molecule technique used for determining the translational diffusion coefficient of fluorescent molecules in a small, sub-femtoliter, volume [46, 47]. The open detection volume is defined by both the microscope objective specifications and continuous wave laser illumination. As molecules diffuse in and out of the observation volume, they undergo excitation-emission cycles. The fluctuations of the emitted fluorescence photons (δF) are detected as a function of time using fiber-coupled avalanche photodiodes (APD). The fiber waveguide acts as a confocal pinhole which also determines the dimensions of the detection volume. The signal from the detected photons is then processed through an auto-correlator device where the fluorescence fluctuation is correlated with itself (i.e., autocorrelation) as a function of the lag time (τ), equation 3.1.

Equation 3.1

$$G(\tau) = \frac{\langle \delta F(t) \delta F(t+\tau) \rangle}{\langle F(t) \rangle^2}$$

Assuming Gaussian excitation and Lorentzian detection profiles, Webb and coworkers [48] derived the corresponding autocorrelation function (equation 3.2) for FCS in terms of the diffusion time (τ_D), structure parameter of the 3D observation volume (S), and number of molecules (N):.

Equation 3.2

$$G_D(\tau) = \frac{1}{N}\left(1 + \frac{\tau}{\tau_D}\right)^{-1}\left(\sqrt{1 + \frac{\tau}{S^2\tau_D}}\right)^{-1} + c$$

Here, translational diffusion is the only cause of fluorescence fluctuation (i.e., the fluctuation of the fluorophore's concentration at nM range). The structure parameter (S) is given by: $S=\omega_z/\omega_{xy}$, where ω_z and ω_{xy} are the axial and lateral extension of the observation volume (Figure 1). Any potential background scattering is expressed by the constant (c), which is known to not correlate. The characteristic diffusion time, τ_D, of a fluorophore can be used to determine the corresponding diffusion coefficient (D) in a given environment using equation 3.3:

Equation 3.3

$$\tau_D = \frac{S_{xy}^2}{N4D}$$

where ω_{xy} is the lateral extension (radius) of the observation volume. In the presence of phosphorescence (or intersystem crossing that causes switching the first singlet excited-state population to the triplet state), however, the corresponding autocorrelation function can be written as (equation 3.3) [49]:

Equation 3.4

$$G_D(\tau) = \frac{1}{N}\left(1+\frac{\tau}{\tau_D}\right)^{-1}\left(\sqrt{1+\frac{\tau}{S^2\tau_D}}\right)^{-1}\left(1+\left(\frac{f_3}{1-f_3}\right)e^{-\tau/\tau_3}\right)+c$$

where f_3 is the population fraction residing in the triplet state with a characteristic lifetime of by τ_3 (i.e., the phosphorescence lifetime).

When a fluorophore diffuses in a heterogeneous environment such as macromolecular crowding, the corresponding autocorrelation function measured using FCS is given by equation 3.5:

Equation 3.5

$$G(\tau) = \frac{1}{N}\left(\frac{1}{1 + \left({}^{\tau}/_{\tau_1}\right)^{\alpha}}\right) + c$$

This empirical equation describes anomalous (non-Brownian) diffusion. The exponent (α) describe the degree of deviation from Brownian diffusion where $\alpha=1$ for Brownian diffusion and $\alpha<1$ for anomalous sub-diffusion.

3.5.2 Experimental setup

The home built system used in the experiments (Figure 3.1) consisted of a fiber-coupled solid-state CW laser (488 nm) (Coherent) which illuminated samples on an inverted microscope (IX81, Olympus). The epifluorescence is then filtered through a 525nm/30nm filter (Chroma) onto 50 μm optical fiber prior to being detected by an avalanche photodiode, APD (spcm-CD 2969, Perkins Elmer). The APD signal is processed via an ALV/6010-160 external multiple-tau-digital correlator (Langen/Hessen). The size of the detection volume is determined using RhG with a known diffusion coefficient. FCS Data is analyzed with OriginPro software. All curves were fit using the Levenberg-Marquardt algorithm, with equations 3.2 or 3.4.

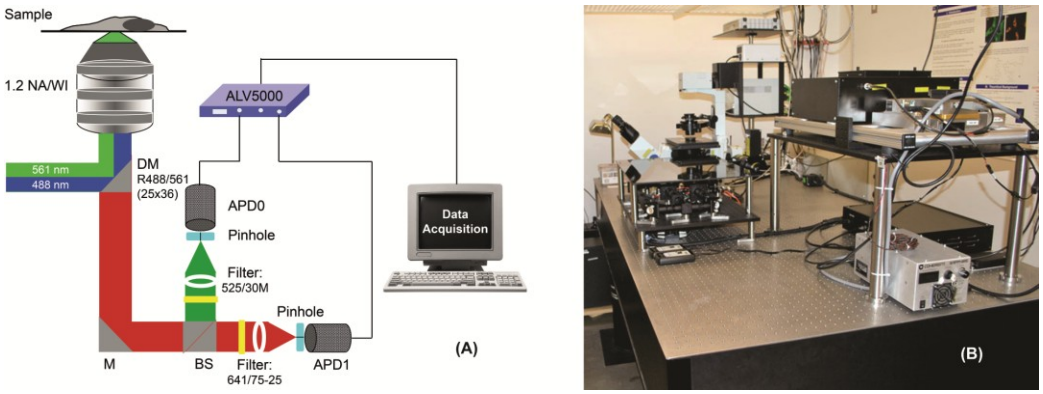

Figure 3.1 (A) Diagram of lights paths for our FCS set up. (B) The homebuilt FCS system

3.6 Time-correlated single photon counting (TCSPC) technique

3.6.1 Fundamentals of TCSPC

TCSPC allows for very precise (picosecond) measurements of the excited-state dynamics and fluorescence lifetime measurements [39]. In these measurements, the fluorophore is usually excited by pulsed laser (femtosecond to picosecond pulse width) at low repetition rate (e.g., 4.2 MHz) such that each pulse will find the fluorophore in the same initial conditions. In TCSPC, however, only a single photon is detected in each excitation-detection cycle and its arrival time is recorded. The excitation-detection cycle is repeated many times and a histogram of the probability of photon detection as a function of its arrival time is recorded, which represent the fluorescence decay (Figure 3.2) of the fluorophore under investigation.

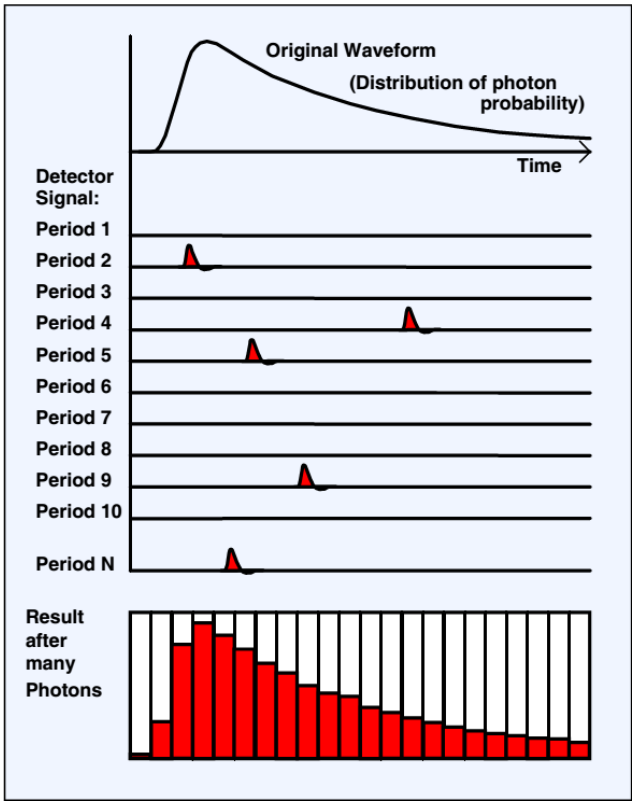

Figure 3.2 A visual description of TCSPC photon probability distribution. Reproduced with permission from The bh TCSPC Handbook figure 104 page 52 [50]

3.6.2 Experimental setup

The experimental setup (Figure 3.3) used for fluorescence lifetime and anisotropy measurements, based on TCSPC technique, has been described elsewhere in detail [51, 52]. A horizontally polarized, femtosecond pulsed laser (76 MHz, ~120 fs pulses, 950 nm), was generated with a Mira 900-F titanium sapphire laser system (Coherent). A Mira 9200 acousto-optic pulse picker (Coherent) was used to reduce the laser repetition rate to 4.2 MHz used in these measurements. A small fraction (<5%) of the laser beam was reflected into a fast photodiode (PHD, Becker and Hickl) to synchronize the single-photo

counting module (SPC 830) with the laser pulses. For one-photon excitation, the second harmonic was generated using an SHG4500 (Coherent). The beam was then conditioned and steered toward an inverted microscope (IX81, Olympus) for sample excitation via a 1.2NA, 60x, H_2O immersion objective (Olympus). The epifluorescence was then detected via right-hand-side exit port of the microscope, filtered using a 525/30 filter (Chroma), polarization-analyzed using Glan-Thompson analyzer at magic angle, and then detected by a microchannel plate photomultiplier tubes, MCP-PMT, (R3809U, Humamatsu) for fluorescence lifetime measurements [39]. The fluorescence decay was then recorded using SPC 830 module (Becker and Hickl) and analyzed using SPCM software (Becker and Hickl) on a personal computer.

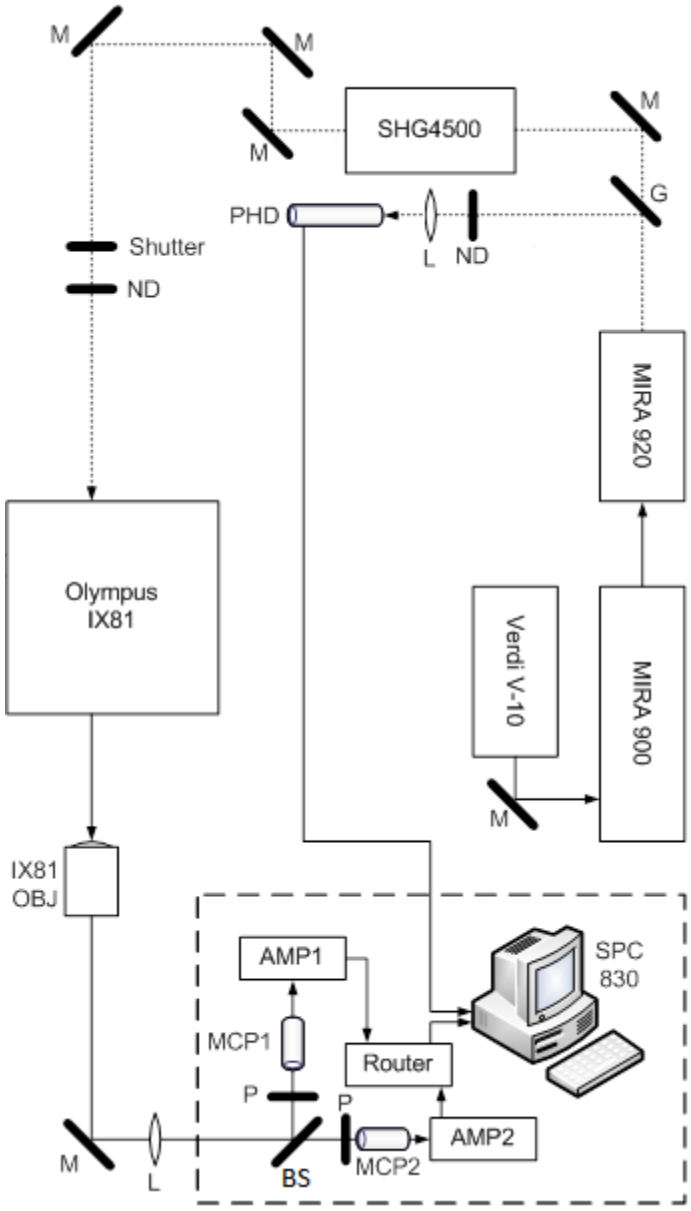

Figure 3.3 Diagram of the TCSPC system. G – glass, M – mirror, L – lens, ND – neutral density filter, SHG – second harmonic generator, BS – beam splitter, AMP – voltage amplifier, PHD – fast photo diode.

3.6.3 Fluorescence lifetime measurements

The fluorescence lifetime of a given fluorophore depends on its chemical structure, its local environment (e.g., refractive index, viscosity), and binding with other molecules). As a result, the nature of the corresponding fluorescence decay can be a simple exponential decay or multi-exponential. Lifetime decays are influenced by a number of factors such as the chemical structure of the fluorescent molecule, refractive index of solution, and interactions between the molecule and its environment. We measured the time resolved fluorescence lifetime by measuring the fluorescence intensity decay, like the one pictured in figure 3.2, the decay can be fit to equation 3.6 [39].

Equation 3.6

$$I_{54.7}(t,x,y) = \sum_{i=1}^{2} \alpha_i(x,y) \cdot e^{-t/\tau_i(x,y)}$$

Where the time constants, τ_i, and the amplitude(s), α, are used to calculate the fluorescence life time.

Equation 3.7

$$\langle \tau_{fl} \rangle = \frac{\sum_{i=1}^{2} \alpha_i \tau_i}{\sum \alpha_i}$$

Lifetime data was analyzed with the SPCIMAGE software from Becker and Hickl. Fluorescence intensity decays were fit with single or bi-exponential decay functions using the non-linear least squares method.

3.6.4 Time-resolved anisotropy measurements

Time-resolved fluorescence anisotropy allows for real-time monitoring of the rotational (tumbling) motion, i.e. rotational diffusion, of a fluorescent species. This was achieved by using the same experimental setup described above (Figure 3.2) for lifetime measurements with a minor modification. For example, the parallel and perpendicular polarization components of the epifluorescence were separated using a polarizing beam splitter following by Glan-Thompson polarizer for higher polarization selectivity prior to detection by the PMT [39]. In these time-resolved anisotropy measurements, a polarized laser photoselectively illuminates randomly oriented fluorescent molecules (or dipole moments) at time zero (Figure 3.4 A). Molecules with dipole moments with a selective range of orientation with respect to the laser polarization will be efficiently excited. The excited molecules (or dipoles) are then free to rotate in solution at a rate that depends on their size and surrounding environment. Such rotational motion of the excited dipoles will emit depolarized fluorescence photons. The parallel $F_{\parallel}(t)$ and perpendicular $F_{\perp}(t)$ fluorescence polarization, with respect to the laser polarization, are then separated and detected simultaneously.

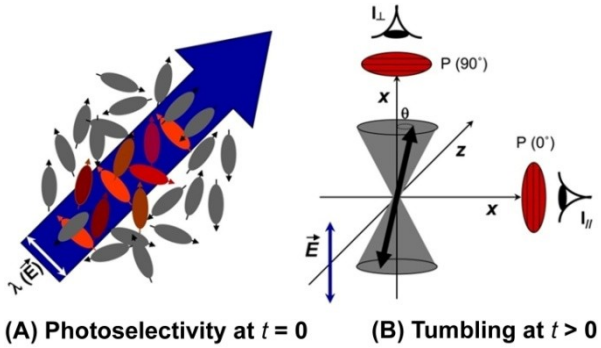

Figure 3.4 (A) Diagram showing how only molecules having the correct orientation become excited by a polarized light source. (B) Diagram showing how the 2 polarizations of fluorescence relates to the orientation of excited molecules.

The time-resolved anisotropy, r(t), was calculated (equation 3.8) using the measured parallel $F_{\|}(t)$ and perpendicular $F\perp(t)$ fluorescence polarizations as follow.

Equation 3.8

$$r(t) = \frac{[I_{\|}(t) - G.I_{\perp}(t)]}{[I_{\|}(t) + 2.G.I_{\perp}(t)]}$$

The G-factor accounts for the potential biased detection of polarized light by the detectors and is determined by a tail-matching approach [39]. Depending on the shape of a fluorescent molecule and its environment the time resolved anisotropy decay can be described by equation 3.9.

Equation 3.9

$$r(t) = \sum_{i=1}^{3} \beta_i \cdot e^{-t/\varphi_i}$$

Where β_i is the amplitude of a given anisotropy decay component and ϕ_i is the corresponding rotational time. A single exponential decay occurs when the rotating molecule is spherical and has no interactions with its environment (e.g., a photostable fluorophore in a buffer). Additional exponential decay components can arise from the molecule being non-spherical, or by the fluorophore not acting as a rigid rotor in respect to the diffusing species as a whole. The rotational time of a given species is directly related to its hydrodynamic volume (V) as well as the viscosity (η) of the surrounding environment (or, ultimately, crowding) such that:

Equation 3.10

$$\varphi = \frac{\eta V}{k_B T} \equiv \frac{1}{6D_R}$$

where k_B and T are the Boltzmann constant and temperature, respectively. The rotational time is also related inversely to its rotational diffusion coefficient (D_R). It is worth noting that the average rotational time for a fluorophore with multi-exponential anisotropy decay can be calculated using equation 3.11:

Equation 3.11

$$\theta = \frac{\sum_{i=1}^{N} \beta_i \varphi_i}{\sum_{i=1}^{N} \beta_i}$$

3.6.5 Software development for raw anisotropy data: Reformatting and analysis

The raw time-resolved, polarization-analyzed data obtained from the SPC-830 are saved in a proprietary format (.sdt) and require some adjustment prior to calculating the corresponding anisotropy decays. For example, since the two PMTs are not identical, the baseline of the time-resolved parallel and perpendicular fluorescence polarizations would require normalization (i.e., to be equated) first. In addition, there is minor difference between the zero-time for the fluorescence decay of each detector that has to be adjusted. The processing of these raw data is time consuming, especially with the number of samples investigated in these studies. Such time consumption becomes problematic considering the number of crowding agents (type and concentration), fluorescent probes, and experimental repetition for standard-deviation analysis and reproducibility tests. As a result, a software program was developed, using the LabView® (National Instruments) framework, allows for directly reformatting and adjusting the parallel and perpendicular polarization prior to anisotropy decay calculations and analysis. In addition, the software enabled us to estimate the G-factor using the polarization analyzed decays and tail-matching approach [39]. The outcome of this program (Figure 3.3) was formatted (.txt) such that it can be directly fed to OriginPro for non-linear least-square fitting (equation 3.9) using the Levenberg-Marquardt algorithm. For more details on this program and its step-by-step operation, please see Appendix I.

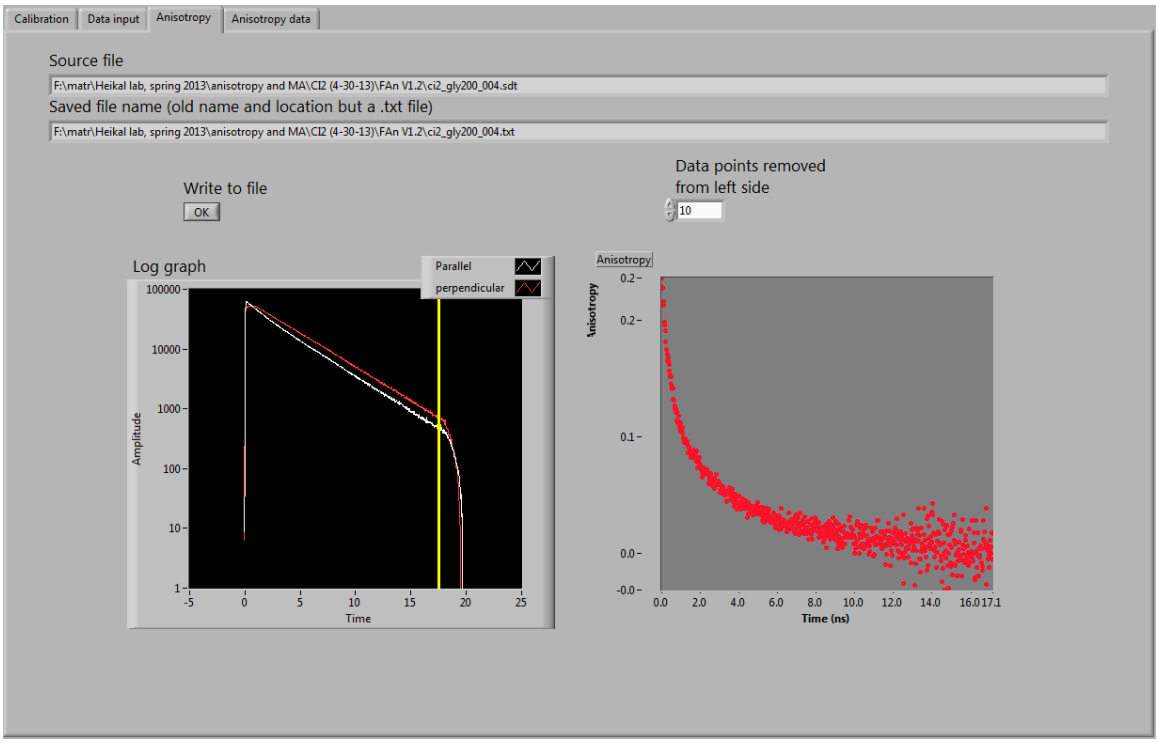

Figure 3.5: A screenshot of the LabView-based program that was developed for reformatting and adjusting both the time-zero and baseline differences between the two parallel and perpendicular fluorescence decays.

Chapter 4: Crowding Effects on Translational Diffusion as Revealed by Fluorescence Correlation Spectroscopy

4.1 Introduction

Fluorescence correlation spectroscopy (FCS) is a single-molecule technique for determining the diffusion coefficient and number of molecules of fluorophores in an open, optically-defined observation volume (Chapter 3). The same approach has been used to investigate crowding effect on diffusion using a wide range of fluorescent probes and crowding agents [3, 11, 25, 30, 53]. In those FCS-based studies, diffusion mechanisms and therefore fitting function (equation 3.5) have been used such as anomalous diffusion mechanism [25, 32]. As for the crowding agents, a wide range of synthetic and biological macromolecules were used to create crowded environments (including live cells) [3, 30]. In addition, different data analysis algorithms were also employed for data interpretation [11, 31]. There, as yet, is no consensus on the effect of molecular crowding on translational diffusion, with different groups citing anomalous diffusion [25, 30], multiple discrete microviscosities [11], or even no discernable change from Brownian motion with FCS [4].

Pielak and co-workers have also investigated translational and rotational diffusion coefficients of CI2 using PFG NMR in some of the same crowded environment as our experiments [5, 6, 34]. Their results were discussed in terms of macroviscosity and microviscosity of crowded environments. However, the molecular concentration needed for NMR studies is in the millimolar range as compared with the nanomolar range for

FCS. The temporal resolution of NMR-based studies, however, is inherently slow (milliseconds to seconds) [38] as compared with sub-microsecond resolution in FCS [49]. In addition, NMR requires a low pH environment which is significantly lower than the physiological pH. NMR looks at displacements of 10-100 nm but does so for a large ensemble of molecules, FCS can have single molecule sensitivity, but the displacement range is limited to the radial component of the detection volume >200 nm for our experiments.

As a result, the inherent global averaging in FCS is significantly lower than NMR which provides a unique opportunity for using single-molecule probes in crowded environments in the μs-ms temporal range. With these differences in mind, direct comparison between NMR and FCS studies on crowding effects on diffusion is rather critical to elucidate the length and temporal scaling associated with diffusion in a crowded environment. The primary difference between those studies and the one reported in this chapter is the context of microviscosity versus macroviscosity in data interpretation, with some exception [11]. In addition, the experimental design reported here aimed at bridging the gap between different experimental techniques such as FCS and NMR [6] as well as fluorescent probes and crowding agents of different sizes. Finally, these FCS studies are complemented by time-resolved anisotropy on the same molecular systems to elucidate the spatio-temporal scaling associated with crowding.

In this chapter, we investigate the nature of translational diffusion of multiple fluorescent tracers in controlled crowded environments and compared with a viscous continuum. RhG, EGFP and CI2 were used as diffusing tracers to assess the size and chemical structural effects of crowding on translational diffusion. Using FCS, the translational diffusion coefficient of these fluorophores was measured in buffers crowded with Ficoll 70, Ficoll 400, ovalbumin, and BSA at room temperature. The results are compared with a continuum created by buffer-glycerol mixture at variable concentrations and macroviscosity. With mixing, the pH of the buffer was chosen to be pH7.6. However, at the highest concentration used in these studies, the pH of the crowded environment at the highest concentration of ovalbumin, BSA, and glycerol was reduced than the pure buffer. These reduced pH values at the highest end of crowding-agent concentrations remain at or above the isoelectric point of EGFP and CI2.

Such comparison is essential to assess the microviscosity (please see appendix II for a detailed explanation of microviscosity) that is created by crowding agents and probed with FCS with respect to the macroviscosity. The material and methods used in this chapter are described in Chapter 3. For a molecule undergoing a Brownian diffusion, the normalized diffusion coefficient with respect to that in a buffer (D_w/D_c) is expected to be linearly dependent of the corresponding viscosity ratio (η_c/η_w), Equation 4.1, as shown schematically in Figure 4.1.

Equation 4.1

$$\frac{D_{water}}{D_{crowded}} = \frac{\eta_{crowded}}{\eta_{water}}$$

If the translational diffusion of a given particle deviates from the SE model, then the above mentioned ratios will deviate from linearity (Figure 4.1).

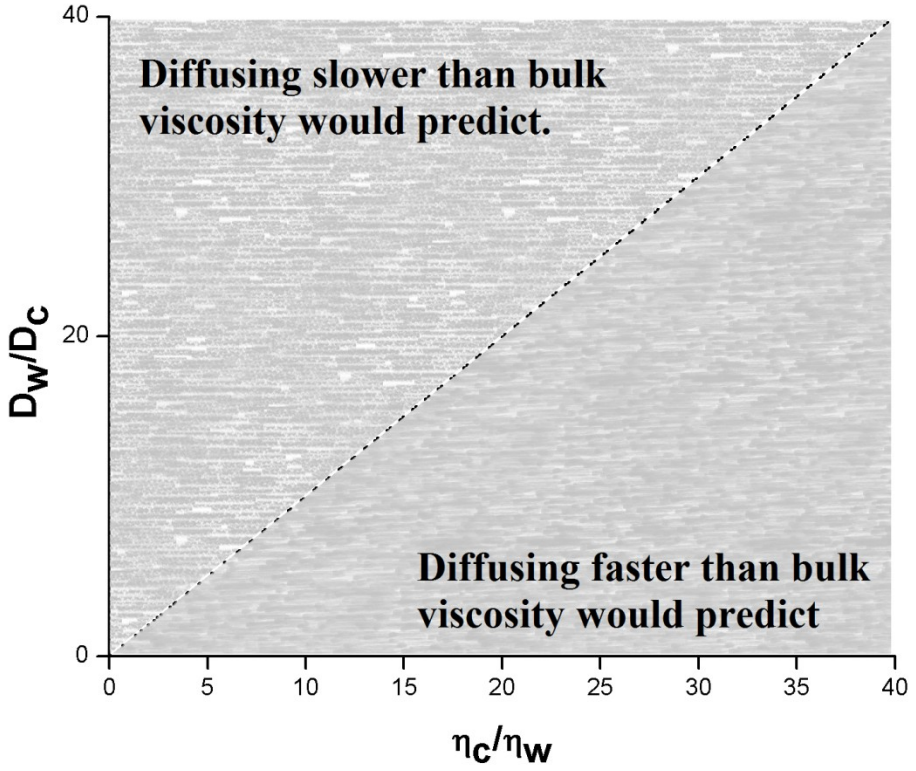

Figure 4.1 Example of D_w/D_c versus η_c/η_w plot, highlighting where and what type of deviations from SE and SED equations are.

According to Stokes-Einstein model, the translational diffusion coefficient measured using FCS depends inversely on viscosity. As a result, we used FCS to determine the viscosity of the local environment sensed by the fluorescent tracer while it diffused. Microviscosity, as measured by FCS, was compared with the macroviscosity, determined by an Ubbelohde viscometer to discover potential differences between macroviscosity

and microviscosity as well as potential non-specific binding between tracers and crowding agents.

4.2. Observation volume calibration in pure buffer

Figure 4.2 shows typical autocorrelation curves for RhG, EGFP and CI2 in pure buffer at room temperature. In pure buffer at room temperature, the diffusion coefficient of rhodamine green is 280μm^2/s [54], which correspond to a measured diffusion time of ~58 μs under our experimental conditions (confocal pinhole of 50 μm and 1.2NA objective). As a result, the radial extension (ω_{xy}) of the observation volume of FCS setup is estimated (~255 nm) using the equation 3.3.

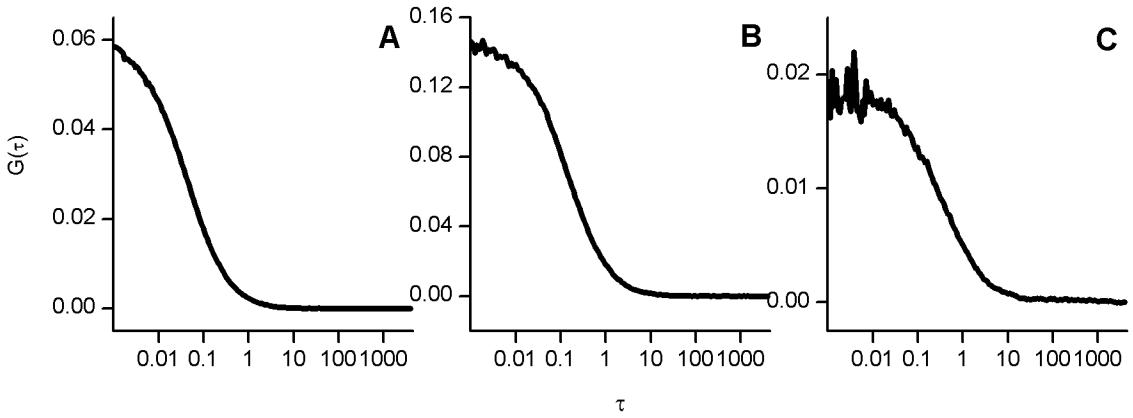

Figure 4.2 Curves generated from FCS on all tracers in PBS. Plot made from the mean of all points generated from autocorrelation function from 20 consecutive scans in black. (A) rhodamine green (B) CI2 (C) EGFP

Such calibrations of the observation volume were carried out on every day of experiments with other fluorescent probes. In addition, the diffusion coefficient of rhodamine green also suggests a hydrodynamic radius of 0.77 nm, which is consistent

with a diffraction-limited focal radius and the molecular mass of the diffusion species (507 Da). Table 4.1 summaries the diffusion coefficient of RhG, EGFP and CI2 in a pure buffer at room temperature. According to Stokes-Einstein model, our results show that the diffusion coefficient decreases as the molecular mass increases (Table 4.1). The molecular mass of EGFP, reported by the supplier (Biovision), is 32.7 kDa which corresponds to 2.29 nm radius assuming a spherical shape. Using the measured diffusion coefficient of 76 ± 10 $\mu m^2/s$ for EGFP in a buffer, in a calibrated observation volume, would yield a hydrodynamic radius of 2.8 nm, which is in close agreement to the 2.82 nm hydrodynamic radius cited in literature [55]. In these calculations, we assumed a 20°C temperature and a water viscosity of 1 cP. By comparison, the fluorescence labeled CI2 has a molecular mass of 7.4 kDa[6] with a calculated radius of 1.4 nm (assuming a spherical shape for simplicity). Using FCS, we estimated a diffusion coefficient of 94 ± 5.3 $\mu m^2/s$, which suggests a 2.28 nm hydrodynamic radius. These results show that the measured diffusion coefficient and hydrodynamic radius are consistent with the molecular mass of EGFP in pure buffer ($\eta \sim$ 1 cP) at room temperature, but are not accurate for CI2 which suggests that either its specific volume and/or hydration is not the same as EGFP or it is not spherical.

Table 4.1: Diffusion coefficients and microviscosities of all tracers in buffer at the highest concentration of crowding agents with FCS, $n \geq 3$ with standard deviation. Bulk viscosities determined by Ubbelohde viscometers n = 3 with standard deviations <1%.

EGFP	Diffusion coefficient $\mu m^2/s$	Bulk viscosity (cP)	Microviscosity (cP)
Buffer	76±10	1	1
Glycerol (900 g/L)	6±1.2	13.14	13.04± 2.69
BSA (300 g/L)	10±21	4.8	7.44± 10.7
Ovalbumin (300 g/L)	7.4±0.63	4.5	9.56± 1.20
Ficoll 70 (400g/L)	3.3±1.4	75.80	27.57± 16.09
Ficoll 400 (400 g/L)	0.80±0.35	248.8	102.41± 44.80
Rhodamine green	Diffusion coefficient $\mu m^2/s$	Macroviscosity (cP)	Microviscosity (cP)
Buffer	280	1	1
Glycerol (900 g/L)	6.4±0.06	13.14	41.98± 10.70
BSA (300 g/L)	27±27	4.8	15.00± 10.34
Ovalbumin (300 g/L)	31±20	4.5	11.02± 5.76
Ficoll 70 (400g/L)	12±2.3	75.80	24.68± 12.07
Ficoll 400 (400 g/L)	17±3.4	248.8	16.66± 5.66
CI2	Diffusion coefficient $\mu m^2/s$	Macroviscosity (cP)	Microviscosity (cP)
Buffer	94±5.3	1	1
Glycerol (900g/L)	3.5±0.4	13.14	27.20± 2.38
BSA (300 g/L)	9.3±1	4.8	10.39± 1.86
Ovalbumin (300 g/L)	8.1±1.5	4.5	12.11± 2.49
Ficoll 70 (400g/L)	6.8±2.7	75.80	18.56± 6.80
Ficoll 400 (400 g/L)	3.9±1.3	248.8	34.49± 14.68

4.3. Crowding effects on molecular brightness and occupancy of observation volume

As mentioned in Chapter 3, the amplitude G(0) in FCS autocorrelation curve equals to 1/N, where N is the average number of diffusing molecules in the observation volume (assuming the contribution from background scattering, c, is negligible). In addition, the molecular brightness of a diffusing species can be determined by using the average signal (kHz) per molecule residing in the observation volume (i.e., S/N).

The general observation is that the brightness of EGFP and CI2 was higher in pure buffer as compared with that in crowded or glycerol-rich environment. In contrast, the number of molecules of these two probes in pure buffer was smaller than in glycerol-rich or crowded environments. The brightness and number of molecules in RhG seems independent of glycerol used in these studies, which might be attributed to the photo-stability and the pH-independent quantum yield of rhodamine green. It is worth noting that the intrinsic fluorescence of BSA and ovalbumin may contribute to the observed increased number of molecules (N) and the lower brightness due to its low fluorescence quantum yield. Another possibility is that the fluorescence probes may interact (soft interaction or non-specific binding) with the crowding agents, which in return influence the fluorescence properties of these fluorescent tracers. Finally, as the concentration of crowding agents increases, the viscosity and excluded volume will increase. In return, the fluorophore will reside longer in the observation volume, which may leads to photo-bleaching due to the longer exposure to laser illumination (i.e., reduced brightness).

The observed increase in the number of tracers diffusing in the same optically-defined observation volume might be explained in terms of the "excluded volume". From the tracer's perspective, the accessible free volume for molecular diffusion will be reduced at higher concentrations of crowding agents due to the excluded volume. In this case, the tracer would experience a smaller volume (i.e., larger number of molecules). Finally, similar trends were observed in Ficoll-crowded solutions as in protein-crowded environment; albeit there is negligible intrinsic autofluorescence of Ficoll.

4.4. Effects of glycerol-induced viscosity changes on the translational diffusion of fluorescence probes: A continuum

To examine the difference between diffusion of a fluorophore in a continuum versus a crowded environment, we carried out FCS measurements of fluorescence probes in glycerol-rich solutions as a reference point. Representative autocorrelation curves of Rhodamine green, EGFP and CI2 are shown in Figure 4.3 at 900 g/L of glycerol in a PBS buffer. The fluorescence fluctuation autocorrelation of all three probes (RhG, EGFP, and CI2) can be satisfactorily described by 3D autocorrelation functions (Equation 3.2 and Equation 3.4) over the viscosity range investigated here. In addition, the signal to noise ratio of the RhG autocorrelation curves were reasonably high over the viscosity range reported here (1-42 cP). In contrast with RhG, the corresponding autocorrelation curves of EGFP and CI2 consistently exhibit a relatively low S/N ratio as at higher viscosity. At higher concentrations concentration (700 g/L: 13 cP; 900 g/L: 42cP) there were much higher levels of noise (Figure 4.3)

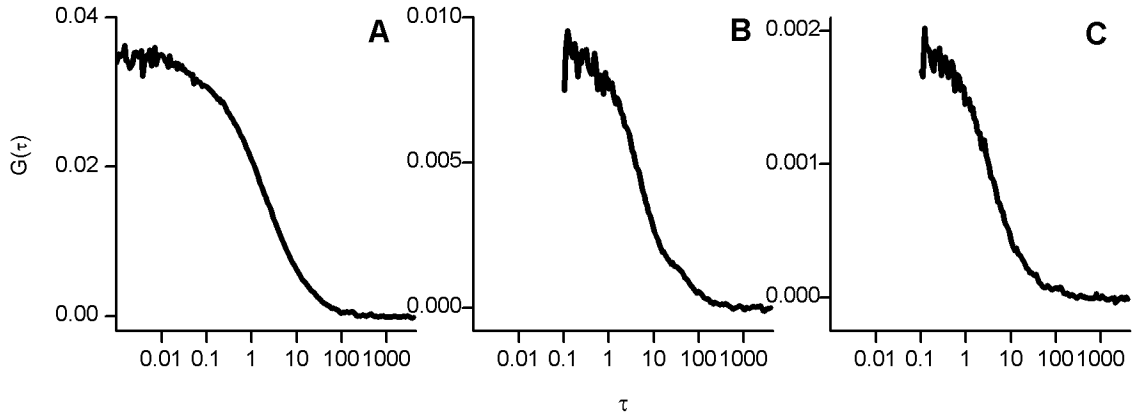

Figure 4.3 Curves generated from FCS on all tracers in 900 g/L glycerol. Plot made from the mean of all points generated from autocorrelation function from 20 consecutive scans in black. Longer diffusion times cause considerable noise in earlier times scales >0.1ms data for the time before 0.1ms has been cut off from CI2 and EGFP curves for clarity. (A) rhodamine green (B) CI2 (C) EGFP

Using the measured diffusion time for each probe in a calibrated observation volume, we calculated the corresponding ratio of translational diffusion coefficient in buffer and that in crowded solutions (D_w/D_c from which the microviscosity, η_c, can be determined by equation 4.1) at different concentrations of glycerol and the results are summarized in Table 4.2. Our results reveal that the microviscosity sensed by RhG, EGFP and CI2 follows the Stokes-Einstein model over a concentration range of 0 g/L to 700g/L (table 4.2). In addition, the diffusion time of RhG increased (i.e. a reduction of the diffusion coefficient) as the bulk viscosity increased as predicted by the SE equation even at the highest concentration.

Table 4.2: Average microviscosity, η_c, values for all tracers in glycerol with standard deviation. n=3 for CI2 and RhG, n=7 for EGFP with standard deviation. . Bulk viscosities determined by Ubbelohde viscometers n = 3 with standard deviations <1%.

Glycerol concentration (g/L)	Bulk Viscosity (cP)	Microviscosity of RhG (cP)	Microviscosity of CI2 (cP)	Microviscosity of EGFP (cP)
0	1	1.00± 0.00	1.00± 0.00	1.00± 0.00
200	2.3	2.57± 0.55	2.58± 0.13	2.59± 0.60
350	3.12	4.37± 0.98	3.86± 0.16	3.78± 0.67
420	4.04	5.28± 1.62	5.06± 0.29	4.54± 0.88
550	6.56	6.83± 2.13	7.71± 2.18	6.36± 0.94
700	13.14	12.51± 4.29	12.35± 0.98	8.67± 0.84
900	42.74	41.98± 10.70	27.20± 2.38	13.04± 2.69

At the highest glycerol concentrations, however, both CI2 and EGFP exhibit a faster rate of diffusion than predicted by the SE equation; for example the SE model predicts that EGFP will have a diffusion coefficient of 1.8 $\mu m^2/s$ instead of the 6±1.2 $\mu m^2/s$ we see. While this behavior has been reported previously using FCS and labeled β-lactamase inhibitor [56], the exact mechanism is unknown with two plausible theories. First, as viscosity increases so does the dwell time of the fluorophores in the detection volume. Long time exposure to laser illumination can cause photobleaching, which lowers the apparent residence time in the detection volume [57, 58]. A second possibility is that high concentrations of glycerol are reducing the specific volume of the proteins which would decrease their hydrodynamic radius [59] and therefore increases their diffusion coefficients. The effects of glycerol stabilizing proteins have been investigated previously [60] and protein unfolding in glycerol-rich solution seems unlikely. Having said that, however, the diffusion time of EGFP and CI2 still increases as the viscosity of solution increased, albeit not as much as the Stokes-Einstein model would predict.

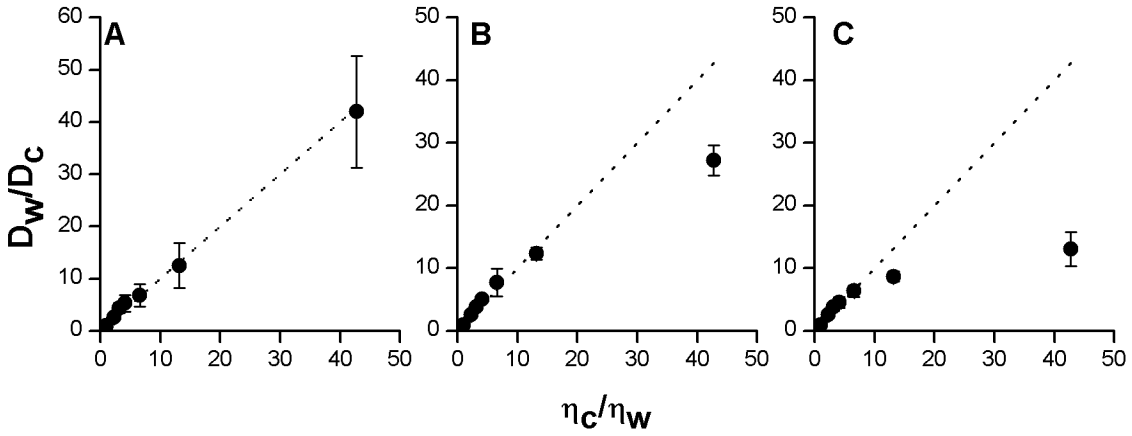

Figure 4.4: Comparison of translational diffusion coefficients in glycerol at various concentrations with all three tracers. All data points are included in table 4.3. (A) rhodamine green (B) CI2 (C) EGFP

The measured diffusion time for each probe was used to calculate the corresponding diffusion coefficient at each viscosity. To examine whether the translational diffusion of each probe can be described by the Stokes-Einstein model, we plotted D_w/D_c as a function of the viscosity ratio η_c/η_w (Figure 4.4). These results indicate that over the macroviscosity range of 1-13 cP, all fluorescence probes investigated here (i.e., RhG, EGFP and CI2) follow the Stokes-Einstein model of diffusion while in a continuum. Such conclusion is in agreement with previous FCS studies on rhodamine green [3], FRAP studies on EGFP [61], and NMR investigation of CI2. [6], which collectively indicate that Stokes-Einstein model is valid for describing the diffusion of these fluorophores in a continuum within the inherent spatio-temporal resolution associated with each technique. In addition, the associated size and chemical structure of these fluorescent probes seem negligible in influencing the diffusion mechanism in glycerol-rich continuum.

4.5 Crowding effects of macromolecules on the translational diffusion of fluorescence probes as revealed by FCS

4.5.1. Ficoll-crowded solutions:

Fluorescence fluctuation autocorrelation curves of RhG, EGFP and CI2 were measured as a function of the Ficoll 70 and Ficoll 400 concentrations at room temperature. These curves are satisfactorily described by 3D autocorrelation function (Equation 3.2) and representative curves are shown in Figure 4.5. In Ficoll-rich solutions, however, spikes in fluorescence fluctuation intensity were observable and the rate of appearance of these spikes increased with the Ficoll concentration. We attributed these spikes to potential aggregate formations between the fluorophore and Ficoll molecules. In our measurements, we used 20 scans for 10 second each and those individual scans that showed distorted autocorrelation curves due to fluorescence spikes were removed prior to data analysis [58]. The magnitude of the distortions increased with the size of Ficoll, its concentration, and fluorophore size as well (Figure 4.5).

The corresponding D_w/D_c ratio was calculated for each fluorophore as a function of the relative viscosity of crowded environment (η_c/η_w) with respect to pure buffer (Figure 4.6). As shown in Figures 4.6 and 4.7, the measured translational diffusion coefficient for all three fluorophores in Ficoll-crowded environment is larger (i.e., smaller D_w/D_c ratio) than predicted by the Stokes-Einstein model. The observed trend with RhG in Ficoll 70 is in agreement with previous studies using FCS [3]. However, Dauty and

Verkman discussed their results in terms of the Ficoll 70 concentration only and without regard to the viscosity according to the Stokes-Einstein model [3]. The authors reported 10-fold increase in the diffusion coefficient of RhG at 400 g/L Ficoll 70. Our results also show that the size of crowding agent affect the crowding-dependent diffusion coefficient as shown in Figure 4.7 for RhG in Ficoll 400. Such comparison between Ficoll 70 and Ficoll 400 provides an direct indication of the size of macromolecules on diffusion mechanisms as well as the heterogeneity of local microviscosity.

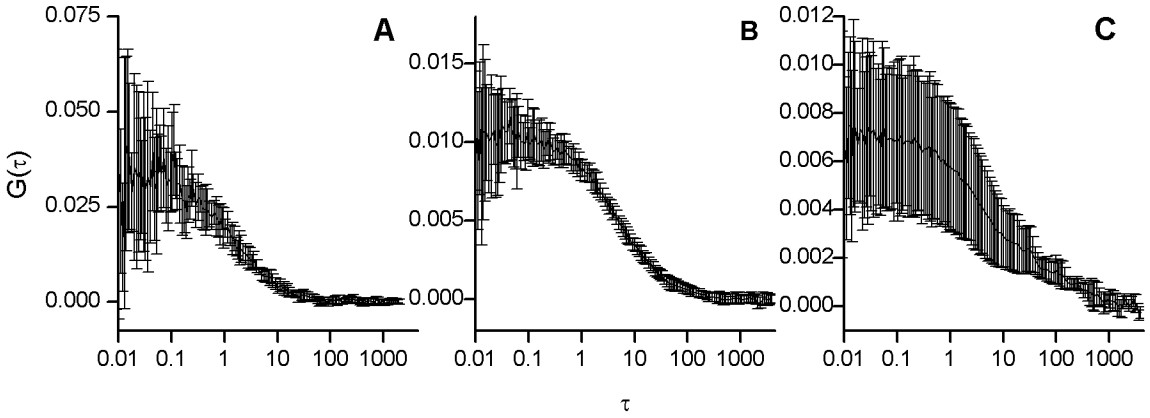

Figure 4.5: Comparison of autocorrelation curves of tracers at 400g/L of Ficoll 400. The plots have been normalized and error bars are in standard deviation. The characteristic distortion is evident at the right tail of the curve. Instead of the tail smoothing out at longer times it fluctuates. (A) rhodamine green (B) CI2 (C) EGFP

The diffusion coefficient of fluorescently-labeled CI2 in Ficoll-crowded solution exhibits a similar deviation from the Stokes-Einstein model, where the measured coefficient was significantly larger than predicted (Figures 4.6 and 4.7). Such observed trend agree with NMR studies on the non-labeled CI2 in an acidic environment of Ficoll 70 [6].

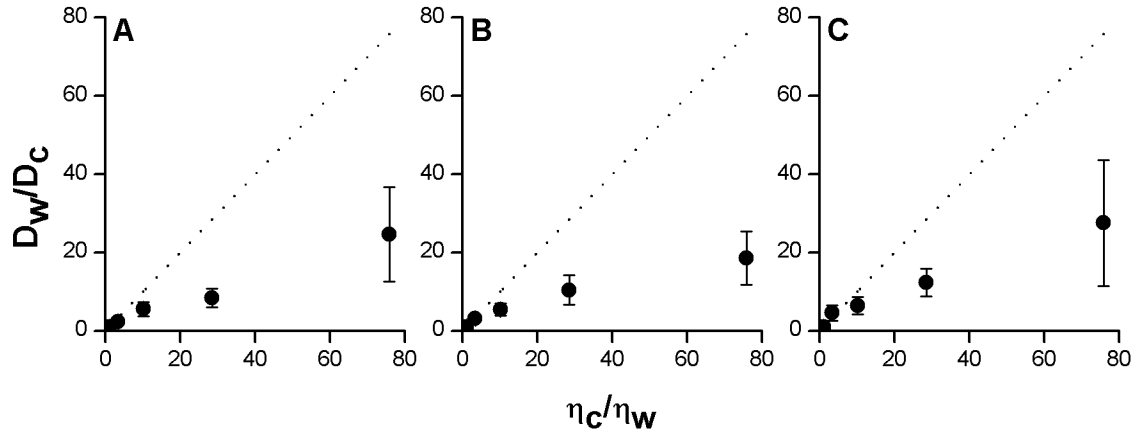

Figure 4.6: Comparison of translational diffusion coefficients in Ficoll 70 at various concentrations with all three tracers. Data points are included in table 44. (A) rhodamine green (B) CI2 (C) EGFP

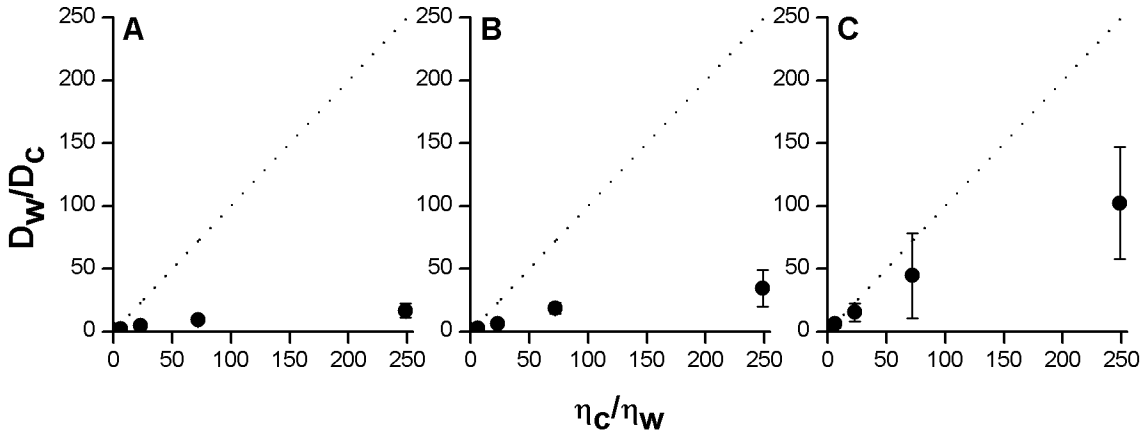

Figure 4.7: Comparison of translational diffusion coefficients in Ficoll 400 at various concentrations with all three tracers. Data points are included in table 4.5. (A) rhodamine green (B) CI2 (C) EGFP

Our results also suggest that Ficoll 70 and Ficoll 400 are likely to form mesh-like networks (i.e., loose its globular shape) at higher concentrations as mentioned in chapter 3. It has been reported that Ficoll form a mesh at concentrations >100g/L [34, 42], which in return may immobilize embedded particles (i.e., causing mush slower diffusion. The larger the diffusing particle the more easily it would be immobilized in the pores of such

a mesh, due to smaller pore sizes being needed to immobilize smaller particles. This perhaps could explain the distortions to the autocorrelation curve. In addition, fluorescence bursts were observed during the recording of the autocorrelation function of EGFP and CI2 at the highest concentration of Ficoll, which in return were removed manually from the averaged scans in order to avoid curve distortion. Aggregate formation between Ficoll and the fluorescent probes, due to non-specific binding for example, may also explain the observed fluorescence bursts as well.

4.5.2. Protein-crowded solutions:

Since proteins are a major component of macromolecules in live cells, we used proteins (namely, BSA and ovalbumin) as crowding agents. These complementary studies in protein-crowded solutions should help us understand how biological (proteins) and synthetic (Ficoll 70 and Ficoll 400) may influence translational diffusion of a fluorophore in crowded environments.

The fluorescence fluctuations of RhG, CI2 and EGFP in protein-rich solutions were satisfactorily described by 3D autocorrelation function (Equation 3.2). The intrinsic background signal of BSA, at high concentrations, was significantly above the background signal. Fluorophore concentration was such that <10% of total intensity was attributable to BSA. In addition, the diffusion time of BSA is ~3 ms there was no effect on the autocorrelation curve at that time in even the highest concentration.

As shown in Figure 4.8, the translational diffusion for RhG, CI2 and EGFP in protein crowded solution was slower (i.e., η_c was higher) than predicted by the Stokes-Einstein model. This deviation is in good agreement in literature for RhG[3] with FCS, CI2 with NMR [6], and no there is no direct comparison was available for EGFP.

These results highlight key differences in diffusion in crowded environment using both biological and synthetic macromolecules. The diffusion of fluorescent probes in Ficoll-crowded environment seems to highlight the excluded volume that is accessible to fluorophores, which explains the observed faster diffusion than predicted by Stokes-Einstein model. In contrast, the fluorescent proteins seem to undergo non-specific binding (or soft interactions; Chapter 2) with proteins in the BSA and ovalbumin-crowded solutions, an argument that agree with literature [6, 27, 62]. Importantly, such non-specific binding seems independent of the chemical structure of the fluorophores used in these studies.

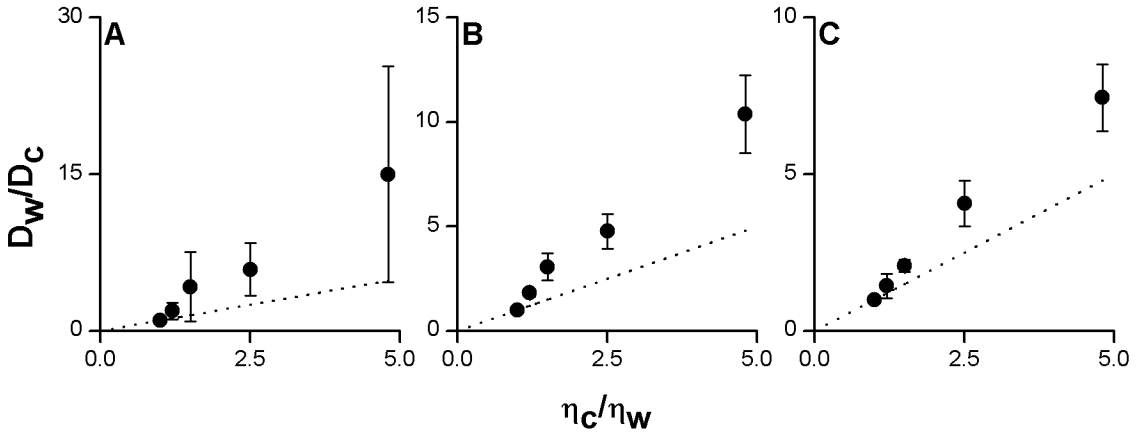

Figure 4.8: Comparison of translational diffusion coefficients in BSA at various concentrations with all three tracers. Data points are included in table 4.6. (A) rhodamine green (B) CI2 (C) EGFP

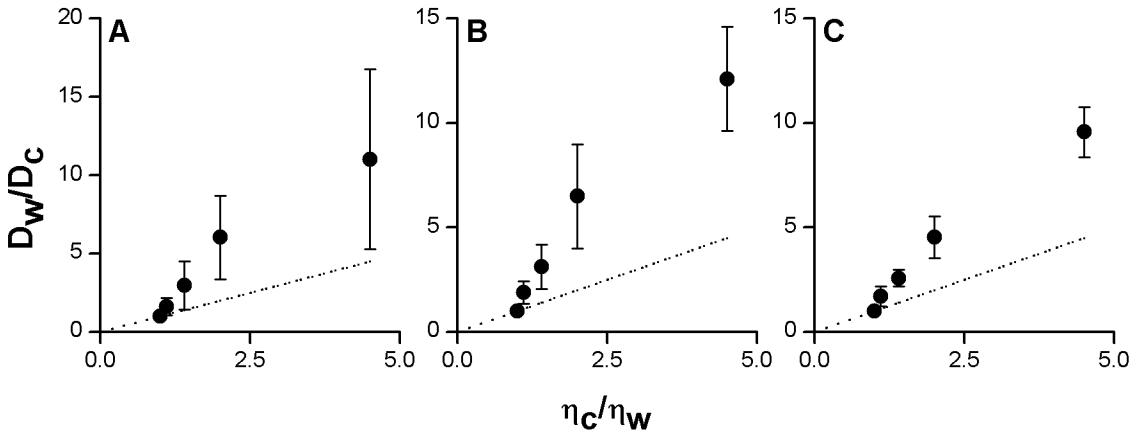

Figure 4.9: Comparison of translational diffusion coefficients in ovalbumin at various concentrations with all three tracers. Data points are included in table 4.7. (A) rhodamine green (B) CI2 (C) EGFP

4.6. Crowding effect of FCS-based microviscosity: comparison with bulk viscosity

Using these FCS results, we examined whether the local viscosity sensed by a fluorophore during its translational diffusion using FCS is the same as the bulk viscosity, measured using a viscometer. Assuming that a given fluorophore investigated here remains monomeric in glycerol-rich solutions, the measured diffusion coefficient was used to calculate the corresponding viscosity during its translational diffusion. In these calculations, we assumed a spherical shape of the fluorophore in Stokes-Einstein model as validated by the above-mentioned Dc/Dw results. Below, we discuss our finding as a function of the glycerol, Ficoll, and protein rich solutions investigated in these studies.

4.6.1. Glycerol-rich solutions:

The calculated microviscosity using FCS data are compared with the bulk viscosity of glycerol rich solution as measured using the viscometer (Table 4.2). These results show that the microviscosity measured using FCS is the same as the bulk viscosity for RhG over the whole range of viscosity (1-42 cP) investigated here. The translational diffusion of CI2 and EGFP in glycerol-rich continuum also reveals a similar trend, except at the highest concentration (900 g/L) of glycerol. The implications of these findings are rather important in investigating diffusion mechanisms, especially in a continuum. The results also demonstrate that translation diffusion of RhG, CI2, and EGFP in a continuum can be described satisfactorily using Stokes-Einstein model. In addition, the diffusing species investigated here sense the same homogeneous viscosity, i.e., the local, microviscosity measured by FCS is the same as the bulk viscosity. Now, the question is whether this conclusion remains valid in crowded environment using synthetic and protein macromolecules, which will be discussed below.

4.6.2. Ficoll-crowded solution:

The results are summarized in Table 4.4 (Ficoll 70) and Table 4.5 (Ficoll 400). In contrast with the glycerol-rich continuum, our results reveal that the microviscosity measured using FCS deviates from the bulk viscosity in Ficoll-crowded environment. Such observation was independent of the fluorescent probe size, but is dependent on the size of the crowding agent (Tables 4.3 and 4.4). As a result, fluorophore are likely to sense local heterogeneity in the viscosity of their surrounding macromolecular-crowded

environment. This conclusion can be understood in terms of excluded volume in the crowded environment.

Table 4.3: Average microviscosity, η_c, values for all tracers in Ficoll 70 with standard deviation. n=3 for CI2, n=3 for RhG, n=6 for EGFP with standard deviation. . Bulk viscosities determined by Ubbelohde viscometers n = 3 with standard deviations <1%.

Ficoll 70 concentration (g/L)	Bulk viscosity (cP)	Microviscosity of RhG (cP)	Microviscosity of CI2 (cP)	Microviscosity of EGFP (cP)
0	1	1.00± 0.00	1.00± 0.00	1.00± 0.00
100	3.36	2.38± 0.83	3.15± 0.77	4.60± 1.93
200	10.12	5.55± 1.76	5.51± 1.56	6.42± 2.18
300	28.47	8.40± 2.41	10.44± 3.82	12.37± 3.49
400	75.8	24.68± 12.07	18.56± 6.80	27.57± 16.09

Table 4.4: Average microviscosity, η_c, values for all tracers in Ficoll 400 with standard deviation. n=3 for CI2, n=3 for RhG, n=4 for EGFP with standard deviation. . Bulk viscosities determined by Ubbelohde viscometers n = 3 with standard deviations <1%.

Ficoll 400 concentration (g/L)	Bulk viscosity (cP)	Microviscosity of RhG (cP)	Microviscosity of CI2 (cP)	Microviscosity of EGFP (cP)
0	1	1.00± 0.00	1.00± 0.00	1.00± 0.00
100	5.98	1.95± 0.51	2.84± 0.93	6.12± 3.01
200	22.9	4.65± 1.72	6.42± 3.15	15.41± 7.26
300	71.95	9.12± 1.85	18.34± 4.35	44.51± 33.64
400	248.75	16.66± 5.66	34.49± 14.68	102.41± 44.80

4.6.3. Protein-rich solutions:

The results are summarized in Table 4.5 (BSA) and Table 4.6 (ovalbumin). In contrast with the glycerol-rich continuum, our results reveal that the microviscosity measured using FCS deviates from the bulk viscosity in protein crowded environment. Such observation was independent of the fluorescent probe size. As a result, fluorophore are

likely to interact non-specifically with the crowding agents which is way the perceived microviscosity is higher than the bulk viscosity.

Table 4.5: Average microviscosity, η_c, values for all tracers in BSA with standard deviation. n=3 for CI2, n=3 for RhG, n=6 for EGFP with standard deviation. Bulk viscosities taken from [6].

BSA concentration (g/L)	Bulk viscosity (cP)	Microviscosity of RhG (cP)	Microviscosity of CI2 (cP)	Microviscosity of EGFP (cP)
0	1	1.00± 0.00	1.00± 0.00	1.00± 0.00
50	1.2	1.92± 0.80	1.81± 0.20	1.43± 0.39
100	1.5	4.22± 3.30	3.06± 0.65	2.08± 0.19
200	2.5	5.88± 2.53	4.76± 0.83	4.07± 0.74
300	4.8	15.00± 10.34	10.39± 1.86	7.44± 10.7

Table 4.6: Average microviscosity, η_c, values for all tracers in ovalbumin with standard deviation. n=3 for CI2, n=3 for RhG, n=6 for EGFP with standard deviation. Bulk viscosities taken from [6].

Ovalbumin concentration (g/L)	Bulk viscosity (cP)	Microviscosity of RhG (cP)	Microviscosity of CI2 (cP)	Microviscosity of EGFP (cP)
0	1	1.00± 0.00	1.00± 0.00	1.00± 0.00
50	1.1	1.62± 0.56	1.90± 0.54	1.70± 0.48
100	1.4	2.97± 1.55	3.12± 1.06	2.56± 0.40
200	2	6.02± 2.65	6.50± 2.49	4.52± 1.00
300	4.5	11.02± 5.76	12.11± 2.49	9.56± 1.20

4.7. Diffusion in biomimetic crowding as compared with that in live cells

Biomimetic molecular crowding has been investigated in the past using Ficoll and proteins [3, 6] to mimic the crowded milieu of live cells. Our results demonstrate the complexity associated with data interpretation associated with translational diffusion of fluorophores in Ficoll crowded environments. In addition, we have shown that synthetic macromolecules (Ficoll 70 and Ficoll 400) differ from that of proteins (BSA and ovalbumin) in their influence on the translation diffusion, perceived microviscosity, and non-specific binding. It is worth noting that the reported viscosity in different

compartments in live cells varies drastically based on the technique or probe used as well as the cellular compartment measurements were made in [63]. For example, a viscosity of ~100 cP is routinely used for biomembranes [64] as compared with ~3-4 cP in mitochondria and ~2.9-3.5 cP for the cytosol[63]. Except at the highest concentrations of Ficoll, the bulk viscosity measured here covers this range as shown in Tables 4.4 & 4.5. Yet, the measured diffusion coefficient in these studies in Ficoll-rich solutions using FCS is faster than that of biomembranes for example (table 4.7 & table 4.1). Accordingly, it is likely that Ficoll rich solutions are unlike the cell environment. For this reason, we discuss proteins as potential crowding agents for biomimetic environment.

Unlike synthetic macromolecules proteins make up a large portion of cellular contents. Also the observed microviscosities in our protein crowded FCS experiments fall in the range observed in cells (table 4.7 & table 4.1). Obviously differences in the exact microviscosity and diffusion coefficients exist based on the structure of the diffusing species, the nature of the crowded environment, and the method used for measurement (as discussed in chapter 2) but the similarities seen between *in vitro* and *in vivo* crowded experiments suggest that proteins make for better biomimics than synthetic macromolecules.

Table 4.7: Diffusion coefficients and calculated microviscosities taken from [63] using FRAP with GFP in CHO E.coli. Diffusion coefficients taken from ECFP taken in PTK2 cells (derived from *Potorous tridactylis*) with FCS (microviscosity not cited).[65]

GFP	Diffusion coefficient $\mu m^2/s$	Microviscosity (cP)	ECFP	Diffusion coefficient $\mu m^2/s$
Water	87	1	Buffer	82±2
Cytoplasm	27.5±2.5	3.2±0.3	Nucleus	20±7
Mitochondria	25±5	3.5±0.5	Cytoplasm	21±8
ER	7.5±2.5	13.5±4.5		

The implications of our findings, concerning the distinct difference between microviscosity sensed by the diffusion molecules as probes by FCS from that of bulk viscosity, are rather important in the crowded milieu of living cells. For example, the measured diffusion coefficient of labeled biomolecules in live cells is likely to be biased by high-affinity association with neighboring proteins or organelles rather than the local viscosity. In other words, FCS-based measurements of cellular viscosity are likely to under estimated, especially in a restrictive cellular environment.

4.8 Summary

The trends of the effect of crowding on microviscosity span all three tracers in continuum and all crowded environments. These same trends are also seen in CI2 in the same solutions, with the exception of Ficoll 400, via NMR. That suggests that the trend of the crowding effect on diffusion is the same for the timescales, spatial scales, pH, and temperature conditions of both methods. It is still very possible that these factors can affect macroviscosity, but just not on the range compared in our two studies.

We have investigated the translational diffusion of size-dependent probes of crowding in glycerol, Ficoll, and protein rich solution using fluorescence correlation spectroscopy. The objective here was to complement time resolved fluorescence anisotropy studies (Chapter 5) to examine the effect of length and time scales associated on diffusion in a crowded environment. Conceptually, translational diffusion of fluorophores is likely to be sensitive to the molecular collisions caused by excluded volume due to the spatial scaling on the microsecond to millisecond time scale. This rationale is true both in the absence and the presence of non-specific binding (or soft interactions) between the fluorescent probes and crowding agents. As a result, our translational diffusion studies are designed to elucidate the role of non-specific binding based on the chemical structure of both the fluorescent probes and crowding agents as well as volume exclusion.

Our results show that translational diffusion in crowded environments deviates from the Stokes-Einstein model in a crowding agent dependent manner. In addition, the local microviscosity sensed is dependent on the chemical structure of the crowding agent. Our results also demonstrate the key differences between Ficoll and proteins as crowding agents in terms of non-specific binding and the propensity to form a meshwork at high concentrations.

Our findings presented in this chapter have a broader impact concerning the use of FCS measurements to investigate the viscosity and intermolecular association in the crowded milieu of living cells.

Chapter 5: Crowding Effects on Rotational Diffusion as Revealed by Time Resolved Fluorescence Anisotropy

5.1 Introduction

Rotational diffusion of fluorophores takes place on the picosecond to nanosecond time scale, depending on the hydrodynamic volume of the diffusing species and environment it is in, and can be quantified using time-resolved fluorescence anisotropy (chapter 3). This real-time approach has been used in molecular and cellular biophysics (see reference [66] for a recent review) in order to elucidate the rotational time, ϕ, of fluorescently-labeled molecules. Recently, macromolecular crowding effects on rotational diffusion of proteins have been investigated using FAn, both in crowded solutions [67, 68] and in living cells [63, 69].

Pielak and co-workers used NMR to investigate the translational and rotational diffusion of CI2 in crowded environment using synthetic macromolecules and proteins as crowding macromolecules[6]. From the perspective of rotational diffusion, these NMR studies showed that the rate of diffusion of CI2 was slowed by non-specific binding with protein crowders and less affected by the increase of viscosity of synthetic macromolecules. However, NMR inherently requires millimolar concentrations of the crowding probe in addition to the limited temporal resolution (milliseconds to seconds) as discussed in section 4.1. Such large ensemble averaging, in both space and time, is likely to washout interesting effects of crowding on rotational diffusion. In contrast, FAn measurements

provide a more noninvasive approach for real-time monitoring of rotational diffusion at low probe concentration (μM) and high temporal resolution (picosecond to nanosecond).

The rotational diffusion of a fluorescently tagged protein, however, is likely to be dominated by tumbling motions of the fluorescent tag rather than the overall rotation of the protein [67]. For example, the AlexaFluor tag we labeled CI2 with is connected via a maleimide group and a 5(CH_2) chain, which allows for the free tumbling of the fluorescent dye independent of rotation of CI2 [39]. In addition to the choice of linker length, fluorophores with longer fluorescence lifetimes are a preferable for longer monitoring times of the rotational diffusion of relatively large proteins [70]. In contrast, the chromophore of EGFP is rigidly embedded in the β-barrel tertiary structure and isolated from the surrounding environment in its folded state [71], which lends itself to being useful in anisotropy studies.

In this chapter, we investigated the effects of macromolecular crowding on the rotational diffusion of different size probes in glycerol, Ficoll, and protein-rich solutions using time-resolved fluorescence anisotropy. The objective here was to complement our FCS studies (Chapter 4) by examining different length and time scales associated with diffusion in a crowded environment. Conceptually, rotational diffusion of fluorophores in the excluded volume between crowding agents is unlikely to be sensitive to a crowding effect due to the limited time scale we observe. This rationale is only true, however, in the absence of non-specific binding (or soft interactions) between fluorescent probes and

crowding agents. As a result, our rotational diffusion studies are designed to elucidate the role of non-specific binding based on the chemical structure of both the fluorescent probes and crowding agents.

5.2 Fluorescence lifetime

The fluorescence lifetime of fluorophores is sensitive to changes in both the chemical structure (e.g., binding, functional group) and the surrounding environment (e.g., pH, viscosity, polarity) [39]. The excited-state lifetime provides the time window where time-resolved anisotropy and rotational diffusion will be monitored [39]. For example, it is believed that the rotational dynamics and hydrodynamic volume of a fluorophore can be determined accurately if the corresponding rotational time is less than 10-fold of the excited state fluorescence lifetime [39]. The Strickler-Berg model predicts that the radiative rate constant of a given fluorophore is directly proportional to the square of refractive index (n^2) of the surrounding environment [72]. In addition, it is known that the radiative (k_r) and non-radiative (k_{nr}) rate constants are related to the fluorescence decay rate (k_{fl}): $k_{fl} = k_r + k_{nr}$. As a result, fluorescence lifetime measurements would allow us to examine effects of crowding on the excited-state dynamics of the fluorescent probes used here (RhG, labeled CI2, and EGFP). Since an increase in crowding agent concentration is likely to enhance the viscosity, refractive index, and the probability of association with the fluorescent probes, we measured the fluorescence lifetime of RhG, labeled CI2, and EGFP as a function of crowding. These measurements were carried out at the magic angle (chapter 3) to remove any rotational effects on the excited state

dynamics [39]. Figure 5.1 and 5.2 summarize the fluorescence lifetime of RhG, labeled CI2 and EGFP as a function of the concentration of crowding agents as compared with glycerol. In pure PBS, the fluorescence of RhG decays as a single exponential with an estimated lifetime of 4 ns (Figure 5.3) as compared with 3.7 ns for labeled CI2 which also exhibit single exponential decay. In addition, the fluorescence of EGFP decays as single exponential with an estimate lifetime of 2.7 ns.

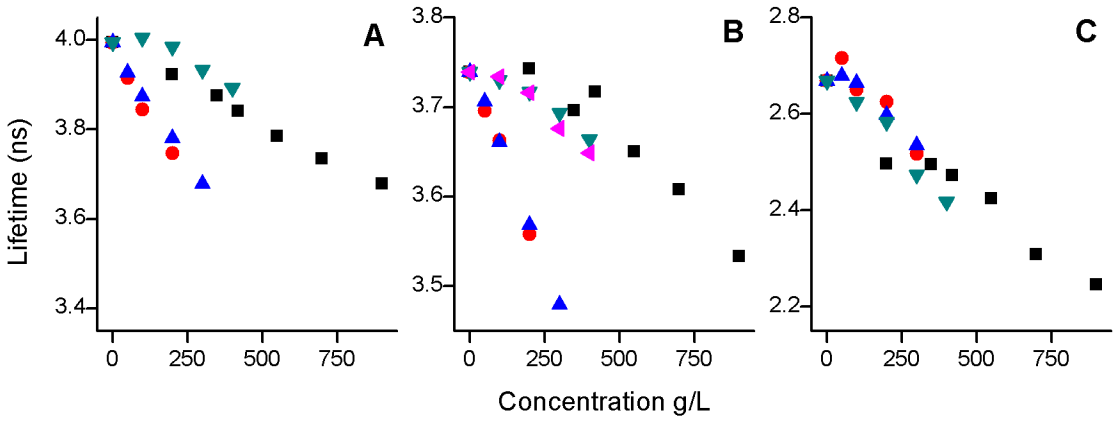

Figure 5.1: Fluorescence lifetime of tracers as a function of crowding (since time-resolved anisotropy depends on the fluorescence lifetime, how crowding affect the fluorescence lifetime). (A) rhodamine green (B) CI2 (C) EGFP. (■) glycerol, (●) BSA, (▲) ovalbumin, (▼) ficoll 70, and (◀) ficoll 400.

In crowded environments, our results show that the fluorescence lifetime of RhG, labeled CI2, and EGFP decreases with the concentration increase of glycerol and the crowding agents (Figure 5.3). In addition, protein crowding seems more effective in reducing the fluorescence lifetime of these probes as compared with glycerol and Ficoll. One possibility is that the observed trend in protein rich solutions may be attributed to non-specific binding with the fluorophores. To examine whether the observed reduction of the fluorescence lifetime can be explained in terms of the changes in the refractive index,

we plotted the fluorescence decay rate as a function of the measured refractive index using an Abbe refractometer (Figure 5.4).

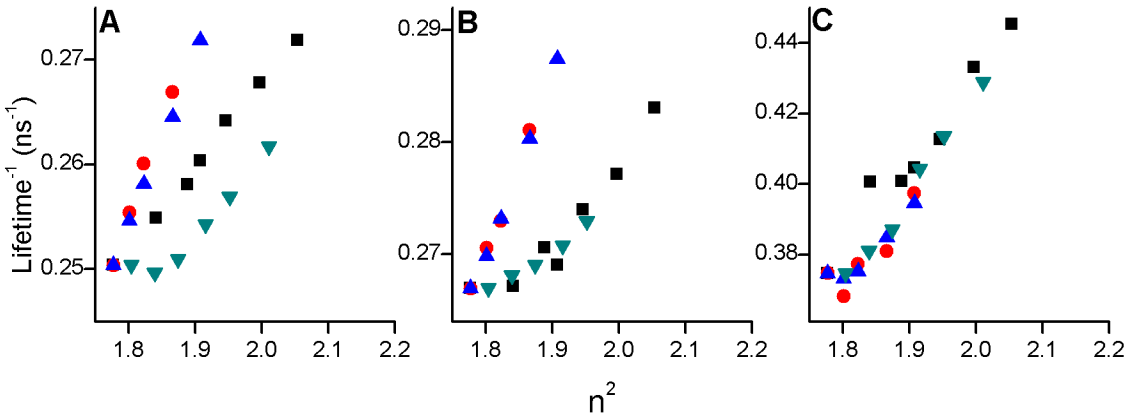

Figure 5.2: Fluorescence rate linearly depends on the square of the refractive of the crowded environment. (A) rhodamine green (B) CI2 (C) EGFP. (■) glycerol, (●) BSA, (▲) ovalbumin, (▼) ficoll 70, and (◄) ficoll 400.

These results reveal that the fluorescence decay rate (the inverse of fluorescence lifetime) is linearly dependent on the square of the refractive index of solution, in agreement with the Strickler-Berg model [72]. The dependence on refractive index of the fluorescence decay rate of RhG and CI2 in protein-crowded environment seems distinct from that of glycerol and Ficoll rich solutions. These results also indicate that the refractive index is more influential in changing the fluorescence lifetime as compared with changes in non-radiative processes. With these results in mind, we now investigate crowding effects on rotational diffusion, starting with buffer as a control.

5.3 Time-resolved anisotropy of RhG, CI2 and EGFP in a continuum: A control

5.3.1 PBS buffer

As a control, the time-resolved anisotropy of RhG, labeled CI2 and EGFP was measured in PBS and the results are shown in Figure 5.3. The anisotropy decay of RhG is a single exponential with a rotational time of ~120 ps at room temperature, which is consistent with its molecular size. In addition, the anisotropy decay of EGFP also decays as a single exponential with a rotational time of 15 ns (Figure 5.3).

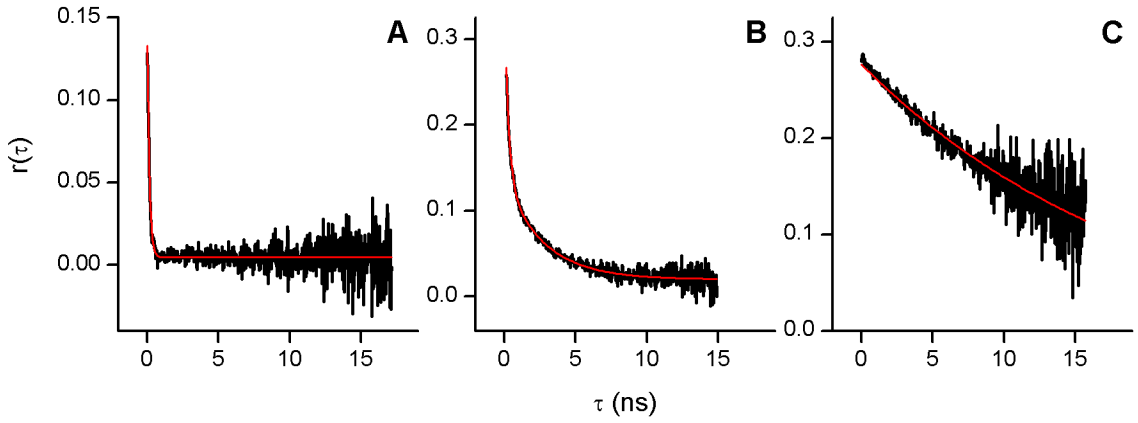

Figure 5.3 Anisotropy curves (with the corresponding fitting curves) of rhodamine green, EGFP, and CI2 in pure buffer at room temperature. The segmental motion of CI2 is evident from the fast decay <5ns and the slow decay at ≥5 ns. (A) rhodamine green (B) CI2 (C) EGFP.

In contrast, the anisotropy decay of the fluorescently labeled CI2 is bi-exponential. The observed bi-exponential anisotropy decay of CI2 indicates that the alexafluor fluorescent tag is free to undergo a segmental motion in addition to the overall rotation of the protein. With these results in mind, we now examine the crowding and glycerol effects on the rotational diffusion mechanism as measured using time-resolved anisotropy.

5.3.2 Glycerol-rich solution:

In accordance with the Stokes-Einstein-Debye model, the rotational time of RhG increases as the viscosity of the glycerol rich continuum increases (Figure 5.4). In addition, a single-exponential decay function satisfactorily describes the anisotropy decay of RhG over the range of concentrations used here. A similar trend was observed for EGFP as well in terms of the glycerol concentration (Figure 4). However, the rotational time of EGFP is significantly slower than the excited state lifetime due to both the molecular weight (~29 kDa) and the increased viscosity at high glycerol concentration. These results are in agreement with previous studies on the rotation of small organic dyes and GFP mutants as a function of glycerol solutions with viscosities <5 cP [71].

In contrast, the bi-exponential anisotropy decay of fluorescently labeled CI2 persists for all concentrations (Figure 5.4). It is worth noting that the continuum's viscosity influenced both the segmental mobility of the fluorescent tag as well as the overall rotational time constant of the CI2-label complex. The viscosity effect on the rotational diffusion of RhG resembles that of the segment mobility of the labeled CI2.

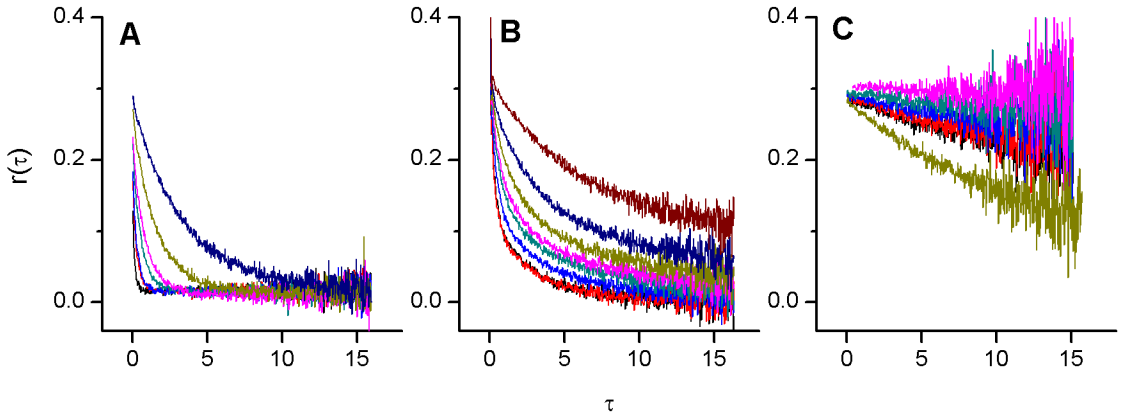

Figure 5.4: Comparison of fluorescence anisotropy decay curves for all tracers in increasing concentrations of glycerol. Curves are in descending order from highest to lowest concentration of glycerol. (A) rhodamine green (B) CI2 (C) EGFP.

To examine the validity of the Stokes-Einstein model in describing the rotational diffusion of RhG, EGFP and labeled CI2 as a function of glycerol concentration, we plotted the rotational diffusion coefficient [39] ratio (D_w/D_c) as a function of the relative viscosity of the glycerol rich solution (η_c/η_w) following our translational diffusion studies in Chapter 4. The results are summarized in Figure 5.5. Over the range of low glycerol concentration, the rotational diffusion of both RhG and EGFP can be described well with Stokes-Einstein model (Figure 5.5). Above $\eta_c \sim 5$ cP, the rotational diffusion of these two probes deviates from the model even in a continuum. Such deviation resembles that observed for the translational diffusion using FCS (Chapter 4). The deviation from the Stokes-Einstein model, however, is more pronounced in the case of the rotational diffusion of the labeled CI2, which (Figure 5.5).

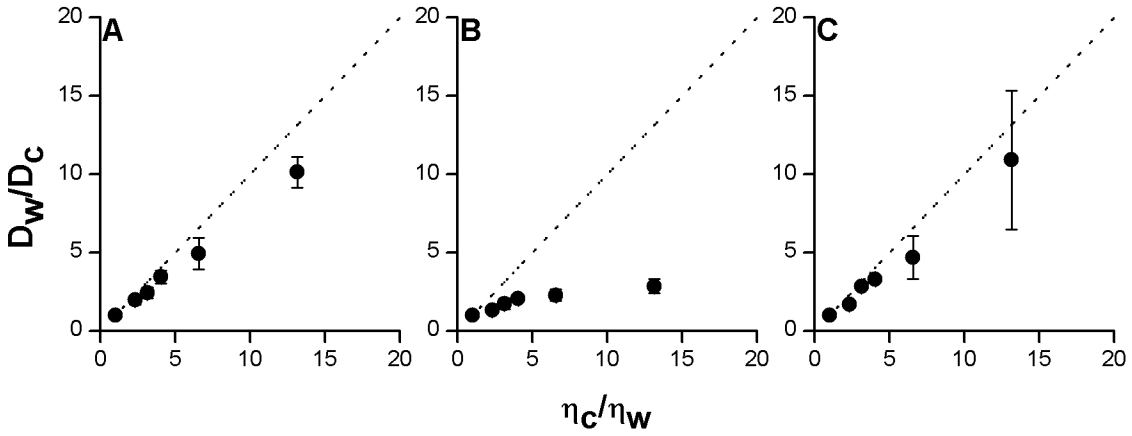

Figure 5.5: Comparison of rotational diffusion coefficients in glycerol at various concentrations with all three tracers. The highest concentration data pointed has been removed for clarity. Data points are included in table 5.1. (A) rhodamine green (B) CI2 (C) EGFP.

The observed deviation from Stokes-Einstein model in the case of RhG and EGFP could be explained by minor laser-induced temperature increase at high glycerol concentration. Such laser-induced temperature changes have been reported previously for IR laser illumination [73]. The bulk viscosity is much more temperature dependent at higher glycerol concentrations [74]. Our results show some agreement with other groups testing microviscosity in glycerol with fluorescence methods [56], especially on the lower range of glycerol concentrations. As for the case of CI2, the observed deviation from this model can be attributed to the complex anisotropy decay due to the segmental mobility of the fluorescent tag with respect to the overall rotation of CI2 peptide. In the rotational diffusion coefficient ratio of CI2, we used the averaged rotational time.

5.4 Macromolecular crowding effects on rotational diffusion of size-dependent fluorescent probes

Conceptually, there are a couple possible scenarios for the time-resolved anisotropy measurements of fluorescent probes in crowded solutions:

(i) **First**, the probes will reside in the gaps in between the macromolecules (e.g., Ficoll or proteins). In this case, the rotational time components for the fluorescent probes should in principles be similar to that measured in pure buffer.

(ii) **Second**, if the fluorescent probes bind (non-specifically or otherwise) macromolecules, then there will be two populations of species in the crowded solution based on the macromolecule concentration; free probes and probes bound to macromolecules. In this case, the anisotropy decay of a given probe is likely to decay as a bi-exponential with a fast time constant as in pure buffer and a slow component that is at least similar to the calculated rotational time of macromolecules.

Below, we examine the rotational diffusion of fluorescent probes in Ficoll and protein crowded environments using time-resolved anisotropy.

5.4.1 Ficoll rich solutions:

Representative time-resolved anisotropy decays of RhG, labeled CI2 and EGFP in PBS are shown in Figure 5.6 as a function of Ficoll 70 concentration (100-400g/L). The anisotropy of EGFP (~29 kDa) decays as a single-exponential with a rotational time of 15-180 ns as a function of the Ficoll 70 concentration. In contrast, the anisotropy of both the RhG and labeled CI2 probes decay bi-exponentially with rotational times increasing

as a function of Ficoll 70 concentration (Figure 5.6). Using the fluorophore rotational times we calculated the rotational diffusion coefficient ratio (D_w/D_c) as a function of the corresponding relative bulk viscosity with respect to the buffer, η_c/η_w, (Figure 5.7). The results show deviation from the Stokes-Einstein-Debye model in a size-dependent manner with respect to the fluorescent probe.

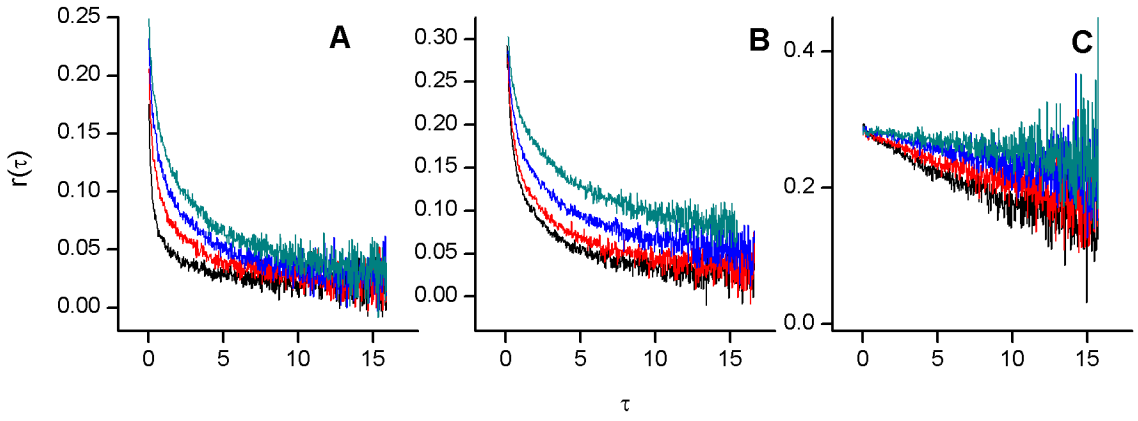

Figure 5.6: Comparison of fluorescence anisotropy decay curves for all tracers in increasing concentrations of Ficoll 70. Curves are in descending order from highest to lowest concentration of Ficoll 70. (A) rhodamine green (B) CI2 (C) EGFP.

The nature of rotational diffusion of RhG in Ficoll 70 depends on concentration of this crowding agent. For example, rotation is slower than is predicted by the Stokes-Einstein-Debye model for lower concentrations (100 and 200 g/L); but plateaus at 300 g/L, where the rotational diffusion becomes faster than expected. This suggests that RhG is associating with Ficoll. Interestingly the microviscosities are within standard deviation of the Ficoll 400 experiments, which is discussed in section 5.5.2.

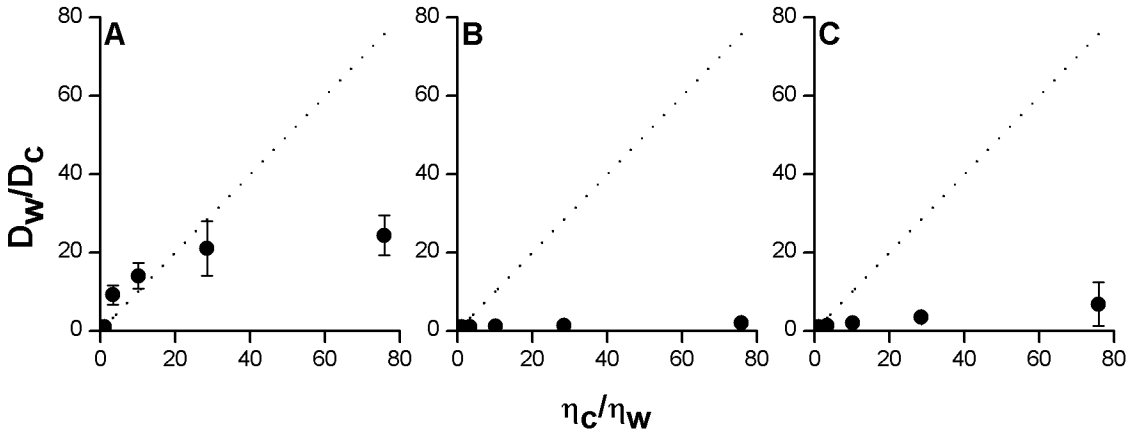

Figure 5.7: Comparison of rotational diffusion coefficients in Ficoll 70 at various concentrations with all three tracers. Data points are included in table 5.2. (A) rhodamine green (B) CI2 (C) EGFP.

In contrast, the rotational diffusion for EGFP in Ficoll 70 rich solution deviates from the Stokes-Einstein model, it diffuses faster than predicted by bulk viscosity, in all concentrations. Accurate rotational times were unattainable for CI2 due to the segmental motion of the fluorescent tag obscuring the rotational motion of the protein.

Similar measurements were carried out on RhG, labeled CI2, and EGFP as a function of Ficoll 400 concentrations to examine the size effect of these neutral polymers on the rotational diffusion on the ps-ns time scale. The results are summarized in Figures 5.8 and 5.9.

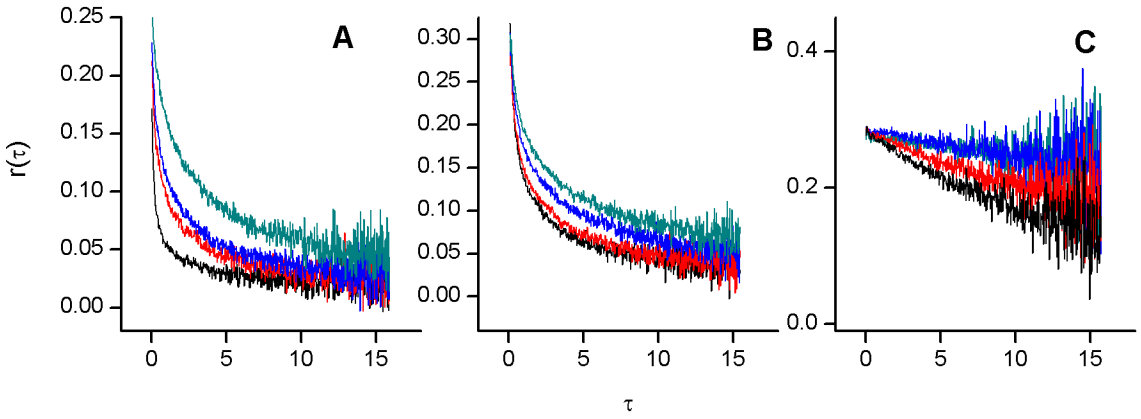

Figure 5.8: Comparison of fluorescence anisotropy decay curves for all tracers in increasing concentrations of Ficoll 400. Curves are in descending order from highest to lowest concentration of Ficoll 400. (A) rhodamine green (B) CI2 (C) EGFP.

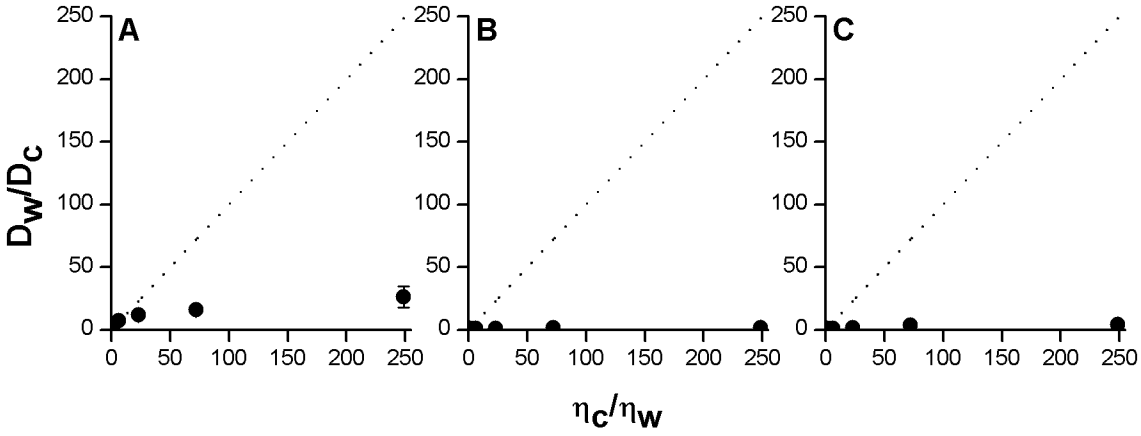

Figure 5.9: Comparison of rotational diffusion coefficients in Ficoll 400 at various concentrations with all three tracers. Data points are included in table 5.3. (A) rhodamine green (B) CI2 (C) EGFP.

The observed trends of anisotropy decays (i.e. rotational diffusion) of these probes in Ficoll 400 generally match those observed in Ficoll 70 crowded solutions (Figure 5.6 & 5.7). These results suggest that some there is some degree of association (non-specific binding) between RhG and Ficoll. The observed deviation from the Stokes-Einstein

model in Ficoll 70 crowded solutions by EGFP is in general agreement with previous studies using NMR measurements CI2 in the same Ficoll 70 concentrations [6].

5.4.2 Protein-rich solutions:

To elucidate the difference between synthetic and protein crowding, we carried out time-resolved anisotropy measurement on RhG, labeled CI2 and EGFP in PBS as a function of BSA (Figure 5.10) and ovalbumin (Figure 5.11) concentrations (50-300g/L). The anisotropy of EGFP (~29 kDa) decays as a single-exponential with a rotational time of 15-75 ns as a function of the BSA (Figure 5.10) and ovalbumin (Figure 5.11) concentration. In contrast, the anisotropy of both the RhG and labeled CI2 probes decays as a bi-exponential as a function of BSA (Figure 5.10) and ovalbumin (Figure 5.11) concentration. Importantly, protein crowding seems to predominantly slow the rotational components of RhG protein-crowded solutions (Figures 5.10 & 5.11).

These results support the above-mentioned second scenario of two populations of free probes in solution and probes bound to those proteins. Conceptually, one would assign the fast rotational component to the free label in buffer-like microenvironment, whose relative population is proportional with the relative amplitude of the fast decay component at a given protein concentration. In contrast, the slow component would represent the probe-protein complex whose relative population is proportional to the relative amplitude of the slow decay component in the anisotropy decay at a given protein concentration.

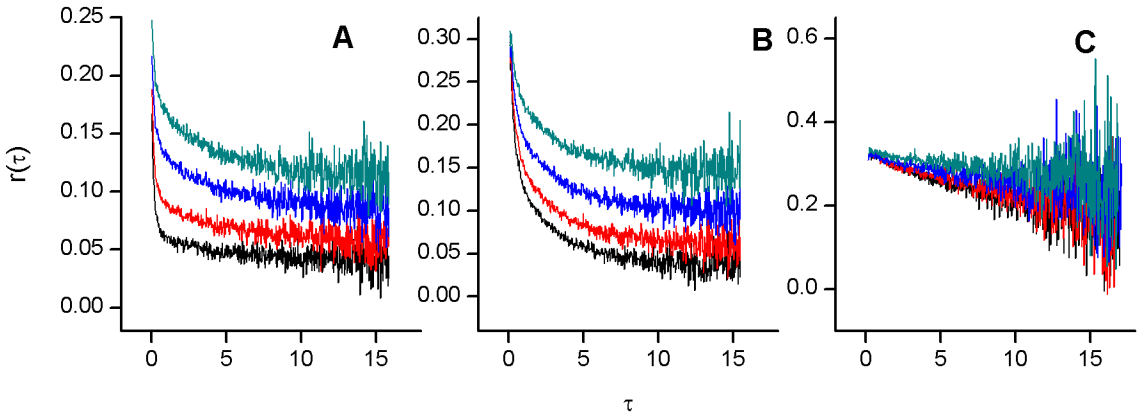

Figure 5.10: Comparison of fluorescence anisotropy decay curves for all tracers in increasing concentrations of BSA. Curves are in descending order from highest to lowest concentration of BSA. (A) rhodamine green (B) CI2 (C) EGFP.

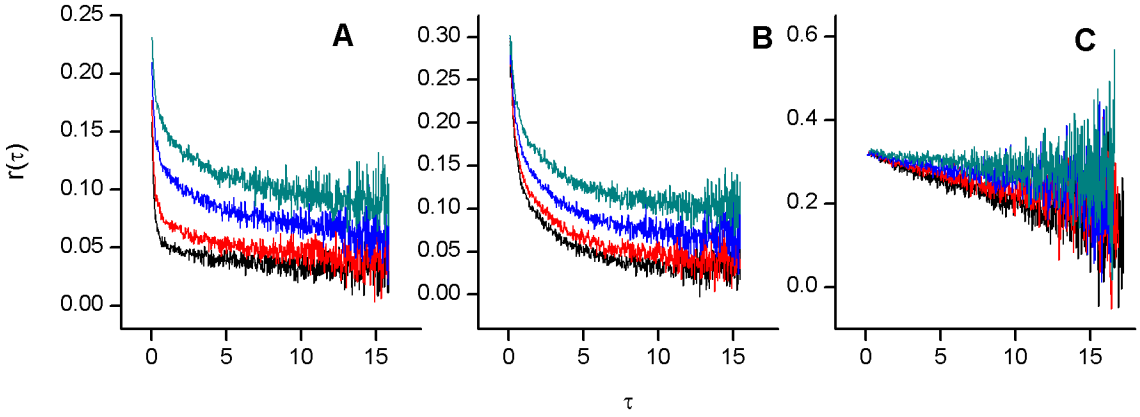

Figure 5.11: Comparison of fluorescence anisotropy decay curves for all tracers in increasing concentrations of ovalbumin. Curves are in descending order from highest to lowest concentration of ovalbumin. (A) rhodamine green (B) CI2 (C) EGFP.

Using the averaged rotational times of these probes, we calculated the rotational diffusion coefficient ratio (D_w/D_c) as a function of the corresponding relative bulk viscosity with respect to the buffer, η_c/η_w, in BSA (Figure 5.12) and ovalbumin (Figure 13) crowded solutions. The results show deviation from Stokes-Einstein model in a probe-dependent manner.

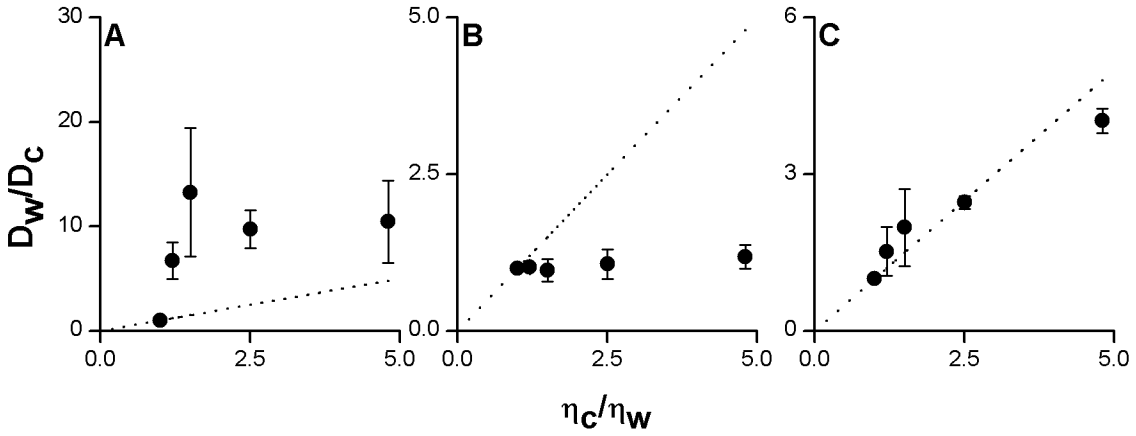

Figure 5.12: Comparison of rotational diffusion coefficients in BSA at various concentrations with all three tracers. Data points are included in table 5.4. (A) rhodamine green (B) CI2 (C) EGFP.

The rotational diffusion of RhG was slower than would be expected by the Stokes-Einstein-Debye equation in terms of bulk viscosity. These results are consistent with RhG interacting, non-specifically binding, with these globular proteins. In contrast, the rotational diffusion of EGFP can be described satisfactorily by the Stokes-Einstein-Debye equation (Figures 5.12 and 5.13). With the inherent limitation in following the rotational diffusion of large proteins using time-resolved anisotropy, these results may suggest a negligible non-specific binding of EGFP with BSA and ovalbumin. In NMR studies, [6] the authors attributed their observed decrease in diffusion rate to soft interactions between their tracer (CI2) and the protein crowding agents in an acidic environment.

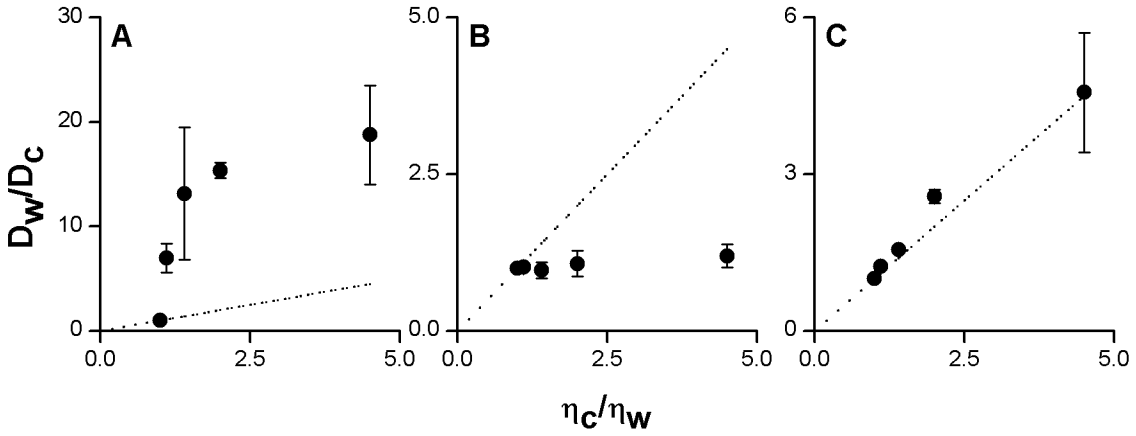

Figure 5.13: Comparison of rotational diffusion coefficients in ovalbumin at various concentrations with all three tracers. Data points are included in table 5.5. (A) rhodamine green (B) CI2 (C) EGFP.

In comparison with our previous FCS results on translational diffusion, which showed a decrease in diffusion rate for EGFP, these time-resolved anisotropy results indicate a dependence on the temporal resolution used in studying macromolecular crowding effect on diffusing species.

5.5 Crowding effects on microviscosity sensed during rotational diffusion: Comparison with bulk viscosity

Using the rotational time measured using time-resolved anisotropy we calculated the corresponding microviscosity in crowded solutions using Ficoll and proteins as compared with a viscous continuum. In these calculations, we assumed that our fluorescent probes remained monomeric without binding with the crowding agents. The bulk viscosities of the crowded solutions were measured using a viscometer (chapter 3). In these calculations, we also assumed a spherical shape of the fluorophore in accordance with the

Stokes-Einstein model. Below, we discuss our findings for RhG, CI2 and EGFP in terms of the crowding agents.

5.5.1 Glycerol-rich solution

The calculated microviscosity using FAn data are compared with the bulk viscosity of glycerol-rich solution as measured using the viscometer (Table 5.1). These results show that the microviscosity measured using FAn is the same as the bulk viscosity for RhG up to 550 g/L. The rotational diffusion of EGFP in glycerol-rich continuum also reveals the same trend.

Table 5.1: Average microviscosity, η_c, values for all tracers in glycerol with standard deviation. n=3 for CI2, n=4 for RhG, n=3 for EGFP with standard deviation. . Bulk viscosities determined by Ubbelohde viscometers n = 3 with standard deviations <1%.

Glycerol Concentration (g/L)	Bulk viscosity (cP)	Microviscosity, RhG (cP)	Microviscosity, CI2 (cP)	Microviscosity, EGFP (cP)
0	1	1.00± 0.00	1.00± 0.00	1.00± 0.00
200	2.3	1.96± 0.27	1.31± 0.22	1.70± 0.18
350	3.12	2.45± 0.35	1.73± 0.36	2.82± 0.13
420	4.04	3.44± 0.40	2.07± 0.23	3.29± 0.18
550	6.56	4.95± 2.01	2.28± 0.37	4.68± 1.38
700	13.14	10.13± 0.98	2.86± 0.44	10.92± 4.44
900	42.74	26.87± 8.77	4.00± 2.00	25.35± 7.55

With the exception of the highest glycerol concentration, the results demonstrate that rotational diffusion of RhG and EGFP in a continuum can be described satisfactorily using the Stokes-Einstein model. In other words, the microviscosity sensed during rotational motion in a continuum is the same as a bulk viscosity. The CI2 results, which deviate from the trend observed for RhG and EGFP can be attributed to the segmental

mobility of the Alexafluor tag obscuring the protein rotational time. Now, the question is whether this conclusion remains valid in crowded environment using synthetic and protein macromolecules, which will be discussed below.

5.5.2 Ficoll-crowded solutions

In contrast with the glycerol-rich continuum, our results (Tables 5.2 & 5.3) reveal that the microviscosity measured associated with rotational diffusion deviates from the bulk viscosity in Ficoll crowded environments. The bulk viscosity is dependent on the size of the macromolecules used to create a crowded environment at the same concentration. For example, the viscosity of Ficoll 400 at 400 g/L is significantly higher than that of Ficoll 70 at the same concentration. The degree of deviation between micro- and bulk viscosity is dependent on the size of the fluorescent probes (Tables 5.2 & 5.3).

Table 5.2 Average microviscosity, $\eta_{c,}$ values for values for all tracers in Ficoll 70 with standard deviation. n=3 for CI2, n=3 for RhG, n=3 for EGFP with standard deviation. . Bulk viscosities determined by Ubbelohde viscometers n = 3 with standard deviations <1%.

Ficoll 70 concentration (g/L)	Bulk viscosity (cP)	Microviscosity RhG (cP)	Microviscosity, CI2 (cP)	Microviscosity, EGFP (cP)
0	1	1.00± 0.00	1.00± 0.00	1.00± 0.00
100	3.36	9.19± 2.44	1.02± 0.04	1.28± 0.10
200	10.12	14.07± 3.36	1.22± 0.16	1.93± 0.23
300	28.47	21.05± 6.96	1.42± 0.30	3.50± 0.64
400	75.8	24.40± 5.05	2.02± 0.29	6.80± 5.56

Table 5.3: Average microviscosity, $\eta_{c,}$ values for all tracers in Ficoll 400 with standard deviation. n=3 for CI2, n=3 for RhG, n=3 for EGFP with standard deviation. . Bulk viscosities determined by Ubbelohde viscometers n = 3 with standard deviations <1%.

Ficoll 400 concentration (g/L)	Bulk viscosity (cP)	Microviscosity RhG (cP)	Microviscosity, CI2 (cP)	Microviscosity, EGFP (cP)
0	1	1.00± 0.00	1.00± 0.00	1.00± 0.00
100	5.98	7.34± 0.65	1.02± 0.04	1.24± 0.14
200	22.9	11.93± 1.66	1.10± 0.19	1.82± 0.13
300	71.95	15.97± 2.93	1.42± 0.35	3.59± 1.31
400	248.75	26.27± 8.67	1.76± 0.32	4.19± 0.57

In addition, the relative microviscosity sensed by a given fluorophore seems dependent on the size of the crowding agent (i.e., Ficoll 70 & Ficoll 400). This observation is consistent with the notion that as the size of the crowding agent increases, tight packing will be reduced, which creates larger gaps between crowding macromolecules with lower, buffer-like viscosity. The relatively small ratio of the microviscosity-to-bulk viscosity sensed by RhG might indicate some degree of non-specific binding with the Ficoll.

5.5.3 Protein-crowded solutions

The microviscosity calculations are summarized in Table 5.4 (BSA) and Table 5.5 (ovalbumin). In both BSA and ovalbumin crowded solutions, our calculations indicate that RhG sensed a higher microviscosity than the bulk viscosity. Considering the small size of RhG, its ability to fill the gaps between macromolecules and small length scale associate with rotational diffusion, these calculations indicate non-specific binding with the proteins.

Table 5.4: Average microviscosity, $\eta_{c,}$ values for all tracers in BSA with standard deviation. n=3 for CI2, n=4 for RhG, n=3 for EGFP with standard deviation. Bulk viscosities taken from [6].

[BSA], (g/L)	Bulk viscosity (cP)	Microviscosity, RhG (cP)	Microviscosity, CI2 (cP)	Microviscosity, EGFP (cP)
0	1	1.0± 0.0	1.0± 0.0	1.0± 0.0
50	1.2	6.7± 1.7	1.02± 0.04	1.5± 0.5
100	1.5	13.3± 6.1	0.97± 0.18	1.98± 0.7
200	2.5	9.7± 1.8	1.1± 0.2	2.5± 0.1
300	4.8	10.4± 3.9	1.2± 0.2	4.03± 0.23

Table 5.5: Average microviscosity, $\eta_{c,}$ values for all tracers in ovalbumin with standard deviation. n=3 for CI2, n=4 for RhG, n=3 for EGFP with standard deviation. Bulk viscosities taken from [6].

[Ovalbumin] (g/L)	Bulk viscosity (cP)	Microviscosit, RhG (cP)	Microviscosity, CI2 (cP)	Microviscosity, EGFP (cP)
0	1	1.0± 0.0	1.0± 0.0	1.0± 0.0
50	1.1	6.98± 1.4	1.02± 0.04	1.24± 0.04
100	1.4	13.1± 6.3	0.97± 0.1	1.55± 0.03
200	2	15.4± 0.7	1.1± 0.2	2.6± 0.1
300	4.5	18.8± 4.8	1.2± 0.2	4.6± 1.2

Such conclusion is in line with the observed bi-exponential decay of RhG anisotropy in protein-rich solutions (Figures 5.10 - 5.13). In contrast EGFP senses the same microviscosity as bulk viscosity. Such observation suggests that the non-specific binding is negligible between EGFP with BSA or ovalbumin, perhaps due to their sizes, or having the same net charge at the buffer the pH (pH 7.6).

5.6 Summary

We have investigated the rotational diffusion of different probes in glycerol, Ficoll, and protein rich solutions using time resolved fluorescence anisotropy. The objective here

was to complement the FCS studies (Chapter 4) to examine the length and time scale associated with diffusion in a crowded environment. Conceptually, rotational diffusion of fluorophores in the excluded volume between crowding agents is unlikely to be sensitive to a crowding effect due to the limited time scale we observe. This rationale is only true, however, in the absence of non-specific binding between the fluorescent probes and crowding agents. As a result, our rotational diffusion studies are designed to elucidate the role of non-specific binding based on the chemical structure of both the fluorescent probes and crowding agents.

Our results show that rotational diffusion in crowded environment deviates from Stokes-Einstein model in a crowding agent dependent manner. In addition, the local microviscosity sensed during the tumbling motion is significantly lower than the bulk viscosity. Our results also show that the increased refractive index of crowded solutions reduces the radiative (or fluorescence) rate of fluorescent probes in a crowding agent dependent manner. This assessment is rather important since monitoring rotational diffusion is limited by the excited-state lifetime, which in turn limits the use of time-resolved anisotropy measurements for quantifying the rotation of macromolecules. Importantly, care must be taken to deconvolute the tumbling motion of fluorescence tags (i.e., segmental mobility of such tags) from that of the overall rotation of the target protein. This emphasizes the importance of engineering fluorescent tags with optimized linker length for accurately measuring rotational motion in and out of living cells. Our

results also demonstrate the key differences between Ficoll and proteins as crowding agents in terms of non-specific binding.

Our findings presented in this chapter have a broader impact concerning the use of time-resolved anisotropy measurements to investigate the viscosity and intermolecular association in the crowded milieu of living cells. In addition, our results raise some concerns regarding the use of rotational-to-translational diffusion coefficient ratio for quantifying the hydrodynamic radius in Stokes-Einstein-Debye model due to the difference in sensed microviscosity during the respective timescales.

Chapter 6: Conclusion and Future Outlook

Using FCS and FAn we have looked at the translational and rotational diffusion of three fluorescent tracers in solutions containing a range of concentrations of various crowding agents. This enabled a comparison between the differences in diffusion caused by size and chemical structure of tracers as well as synthetic and protein crowding agents. The results of these experiments have broadened our understanding of the diffusion on different time and spatial scales.

Our results suggest that the rate of diffusion cannot solely be determined by bulk viscosity and temperature of a solution as well as the size/shape of a diffusing species in said solution as outlined in the Stokes-Einstein and the Stokes-Einstein-Debye models. Diffusion is mediated, in part, by the relationship between size and chemical properties of a diffusing species and other co-solutes (e.g. crowding agents). This relationship cannot be explained purely in terms of excluded volume (i.e. steric repulsion), but also relies on non-specific interactions between molecules in solution. The difference between calculated microviscosities from FCS and FAn suggest that either crowding influences rotational and translational diffusion differently, and/or temporal and spatial boundary conditions affect the rate of diffusion. We have evidence that supports the idea that Ficoll is not entirely globular and the possibility that it forms a meshwork at higher concentrations.

We are the first group to compare rotational and translational diffusion with FCS and FAn of our model systems under the same experimental conditions. This has enabled us to make a good comparison between the rates of rotational and translation diffusion at short time scales. Also we can make a direct comparison of translational diffusion with PFG NMR using the same tracer and many of the same crowders at the same concentrations. Which has suggested that translational diffusion suffers the same crowding affects at those two different time scales (microsecond to millisecond and seconds).

Our results suggest that interpreting changes in diffusion in terms of microviscosities is a good way of looking at heterogeneous diffusion. A different interpretation is to view changes in diffusion through the lens of changes in effective volume of the diffusing species. Both have their roots in Stokes law, but effective volume suggests that effect of bulk viscosity is the same for both translational and rotational diffusion. To calculate the effective radius both the translational and the rotational diffusion coefficients (equations 2.7 and 2.8) are compared as in equation 6.1.

Equation 6.1

$$\sqrt{\frac{3D_t}{4D_r}} = R_{effective}$$

This interpretation seems valid when looking at the results from NMR experiments [6] which determines rotational and translational diffusion on the same time scale. In our

experiments this interpretation seems to hold true for Ficoll and EGFP where we have concluded that molecular collisions are the predominant force effecting diffusion.

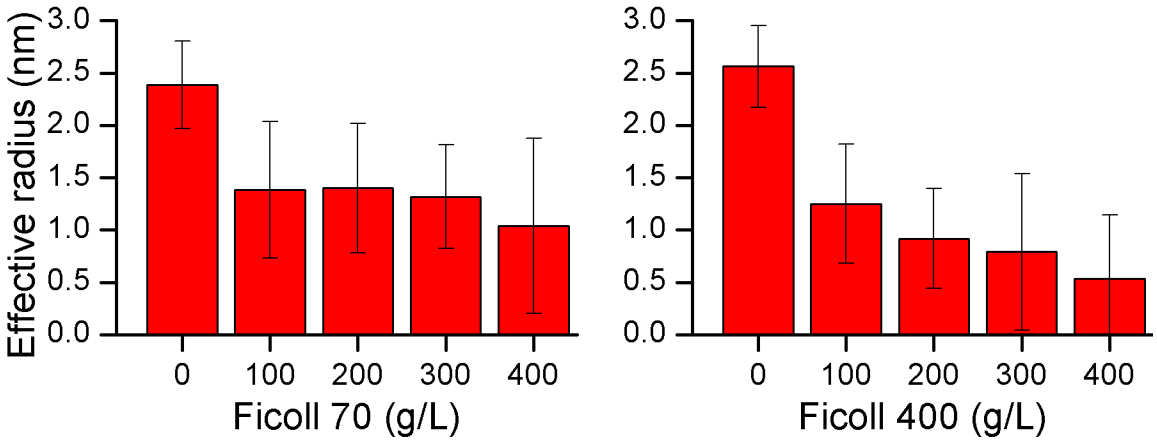

Table 6.1: effective radius with standard deviations of EGFP in different concentrations of Ficoll 70 and 400.

For effective radius change to occur any deviation from the Stokes-Einstein models must be much more pronounced for rotational diffusion, because the Stokes-Einstein-Debye model takes in to account the volume of the diffusing species instead of just the radius (equations 2.7 and 2.8).

There are three main avenues for future studies, looking at new crowding agents, using new fluorescent tracers, and changing solvent conditions. Crowding agents can be roughly broken down in to two camps, synthetic and protein. Synthetic crowding agents are interesting for their uniform surface properties which enable a more pure look at the effect of excluded volume. Up to this point Ficoll has been used, but dextran, and possibly polyvinyl pyrrolidone (PVP) or alcohol (PVA), is appealing because it has not been shown to form a mesh, is available in a very wide range of sizes, and its use by

other groups could lead for enlightening comparison. The protein crowding agents that we have used thus far, while robust, do not represent a very wide range of characteristics. It needs to be borne in mind that the requirements for a good protein include: globular shape, high solubility, purity, and availability for purchase in large quantities (grams). Proteins such as lysozyme and hemoglobin are worth considering.

As for fluorescent tracers options are rather limited. To be a good probe for fluorescence anisotropy the fluorescent moiety must be held rigidly to the diffusing species as a whole. While this is not a problem for some synthetic tracers (e.g. small organic molecules, quantum dots) this proves very problematic for proteins. DSRed and its variants are the only other commonly used fluorescent proteins that meet that requirement, and considering its remarkable similarity to GFP it is not that appealing. Choosing a different fluorescent label with a long lifetime would also assist in accurate FAn measurements. CI2 could be labeled with a different tag as long as it has a thiol reactive moiety that can bind cysteine residues.

The last group of changes involves buffer choice. By changing the pH of the solvent the net charge of proteins can be changed depending on their isoelectric point. It could be interesting to see if an anionic tracer and cationic crowding agent (or vice versa) would amplify the slowing effect on protein diffusion. Changing the ionic strength of the solution could also have an effect on non-specific binding as well.

Bibliography

1. Zhou, H.X., G. Rivas, and A.P. Minton, *Macromolecular crowding and confinement: biochemical, biophysical, and potential physiological consequences.* Annu Rev Biophys, 2008. **37**: p. 375-97.
2. Luby-Phelps, K., *Cytoarchitecture and physical properties of cytoplasm: volume, viscosity, diffusion, intracellular surface area.* Int Rev Cytol, 2000. **192**: p. 189-221.
3. Dauty, E. and A.S. Verkman, *Molecular crowding reduces to a similar extent the diffusion of small solutes and macromolecules: measurement by fluorescence correlation spectroscopy.* J Mol Recognit, 2004. **17**(5): p. 441-7.
4. Dix, J.A. and A.S. Verkman, *Crowding effects on diffusion in solutions and cells.* Annu Rev Biophys, 2008. **37**: p. 247-63.
5. Li, C., Y. Wang, and G.J. Pielak, *Translational and rotational diffusion of a small globular protein under crowded conditions.* J Phys Chem B, 2009. **113**(40): p. 13390-2.
6. Wang, Y., C. Li, and G.J. Pielak, *Effects of proteins on protein diffusion.* J Am Chem Soc, 2010. **132**(27): p. 9392-7.
7. van den Berg, B., R.J. Ellis, and C.M. Dobson, *Effects of macromolecular crowding on protein folding and aggregation.* EMBO J, 1999. **18**(24): p. 6927-33.
8. Vand, V., *Theory of Viscosity of Concentrated Suspensions.* Nature, 1945(155): p. 364-365.
9. Ross, P.D. and A.P. Minton, *Hard quasispherical model for the viscosity of hemoglobin solutions.* Biochem Biophys Res Commun, 1977. **76**(4): p. 971-6.
10. Ross, P.D. and A.P. Minton, *Analysis of non-ideal behavior in concentrated hemoglobin solutions.* J Mol Biol, 1977. **112**(3): p. 437-52.
11. Goins, A.B., H. Sanabria, and M.N. Waxham, *Macromolecular crowding and size effects on probe microviscosity.* Biophys J, 2008. **95**(11): p. 5362-73.
12. van den Berg, B., et al., *Macromolecular crowding perturbs protein refolding kinetics: implications for folding inside the cell.* EMBO J, 2000. **19**(15): p. 3870-5.
13. Helfand, E., et al., *Scaled Particle Theory of Fluids.* The Journal of Chemical Physics, 1960. **33**(5): p. 1379-1385.
14. Saxton, M.J., *Wanted: a positive control for anomalous subdiffusion.* Biophys J, 2012. **103**(12): p. 2411-22.
15. Philibert, J., *One and a Half Century of Diffusion: Fick, Einstein, before and beyond* Diffusion Fundamentals, 2006. **4**: p. 19.
16. Fick, A., *On liquid diffusion.* Journal of Membrane Science, 1995. **100**(1): p. 33-38.
17. Perrin, J.B., *Les atomes*. 1913, Paris: F. Alcan.
18. Kubo, R., *The fluctuation-dissipation theorem.* Reports on Progress in Physics, 1966. **29**(1): p. 255.
19. Einstein, A., *The theory of the brownian movement.* Ann. der Physik, 1905. **17**: p. 549.

20. Koenderink, G.H., et al., *On the validity of Stokes–Einstein–Debye relations for rotational diffusion in colloidal suspensions.* Faraday discussions, 2003. **123**: p. 335-354.
21. Zimmerman, S.B. and A.P. Minton, *Macromolecular crowding: biochemical, biophysical, and physiological consequences.* Annual review of biophysics and biomolecular structure, 1993. **22**(1): p. 27-65.
22. Lemons, D.S. and A. Gythiel, *Paul Langevin's 1908 paper ``On the Theory of Brownian Motion'' [``Sur la th[e-acute]orie du mouvement brownien,'' C. R. Acad. Sci. (Paris) [bold 146], 530--533 (1908)]*. American Journal of Physics, 1997. **65**(11): p. 1079-1081.
23. Bouchaud, J.-P. and A. Georges, *Anomalous diffusion in disordered media: Statistical mechanisms, models and physical applications.* Physics Reports, 1990. **195**(4–5): p. 127-293.
24. Grenier, et al., *Diffusion of methanol in NaX crystals: Comparison of i.r., ZLC, and PFG-n.m.r. measurements.* Zeolites, 1994. **14**(4): p. 242-249.
25. Banks, D.S. and C. Fradin, *Anomalous diffusion of proteins due to molecular crowding.* Biophys J, 2005. **89**(5): p. 2960-71.
26. Ritchie, K., et al., *The fence and picket structure of the plasma membrane of live cells as revealed by single molecule techniques (Review).* Molecular membrane biology, 2003. **20**(1): p. 13-18.
27. Roosen-Runge, F., et al., *Protein self-diffusion in crowded solutions.* Proceedings of the National Academy of Sciences, 2011. **108**(29): p. 11815-11820.
28. Magdziarz, M. and A. Weron, *Anomalous diffusion: Testing ergodicity breaking in experimental data.* Physical Review E, 2011. **84**(5): p. 051138.
29. Metzler, R. and J. Klafter, *The random walk's guide to anomalous diffusion: a fractional dynamics approach.* Physics Reports, 2000. **339**(1): p. 1-77.
30. Weiss, M., et al., *Anomalous Subdiffusion Is a Measure for Cytoplasmic Crowding in Living Cells.* Biophys J, 2004. **87**(5): p. 3518-3524.
31. Szymanski, J. and M. Weiss, *Elucidating the Origin of Anomalous Diffusion in Crowded Fluids.* Physical review letters, 2009. **103**(3): p. 038102.
32. Schwille, P., J. Korlach, and W.W. Webb, *Fluorescence correlation spectroscopy with single-molecule sensitivity on cell and model membranes.* Cytometry, 1999. **36**(3): p. 176-82.
33. Mooney, M., *The viscosity of a concentrated suspension of spherical particles.* Journal of Colloid Science, 1951. **6**(2): p. 162-170.
34. Wang, Y., et al., *Disordered Protein Diffusion under Crowded Conditions.* J Phys Chem Lett, 2012. **3**(18): p. 2703-2706.
35. Lavalette, D., et al., *Microscopic viscosity and rotational diffusion of proteins in a macromolecular environment.* Biophys J, 1999. **76**(5): p. 2744-51.
36. Ellis, R.J., *Protein Misassembly*, in *Molecular Aspects of the Stress Response: Chaperones, Membranes and Networks*, P. Csermely and L. Vígh, Editors. 2007, Springer New York. p. 1-13.

37. White, Andrew D., W. Huang, and S. Jiang, *Role of Nonspecific Interactions in Molecular Chaperones through Model-Based Bioinformatics.* Biophys J, 2012. **103**(12): p. 2484-2491.
38. Kärger, J. and F. Stallmach, *PFG NMR Studies of Anomalous Diffusion*, in *Diffusion in Condensed Matter*, P. Heitjans and J. Kärger, Editors. 2005, Springer Berlin Heidelberg. p. 417-459.
39. Lakowicz, J.R., *Principles of fluorescence spectroscopy*. 3rd ed. 2006, New York: Springer. xxvi, 954 p.
40. Lanni, F., A.S. Waggoner, and D.L. Taylor, *Structural organization of interphase 3T3 fibroblasts studied by total internal reflection fluorescence microscopy.* The Journal of cell biology, 1985. **100**(4): p. 1091-102.
41. Fissell, W.H., et al., *Ficoll is not a rigid sphere.* American journal of physiology. Renal physiology, 2007. **293**(4): p. F1209-13.
42. Rubinstein, M. and R.H. Colby, *Polymer physics*. 2003, Oxford: Oxford University Press. xi, 440 p.
43. Brown, J. *Structure of bovine serum albumin*. in *Fed. Proc*. 1975.
44. Huntington, J.A. and P.E. Stein, *Structure and properties of ovalbumin.* Journal of Chromatography B: Biomedical Sciences and Applications, 2001. **756**(1–2): p. 189-198.
45. Chalfie, M., et al., *Green fluorescent protein as a marker for gene expression.* Science (New York, N.Y.), 1994. **263**(5148): p. 802-5.
46. Hess, S.T., et al., *Biological and chemical applications of fluorescence correlation spectroscopy: a review.* Biochemistry, 2002. **41**(3): p. 697-705.
47. Ries, J. and P. Schwille, *Fluorescence correlation spectroscopy.* Bioessays, 2012. **34**(5): p. 361-8.
48. Maiti, S., U. Haupts, and W.W. Webb, *Fluorescence correlation spectroscopy: Diagnostics for sparse molecules.* Proceedings of the National Academy of Sciences, 1997. **94**(22): p. 11753-11757.
49. Schwille, P. and E. Haustein, *Fluorescence correlation spectroscopy.* A tutorial for the Biophysics Textbook Online (BTOL). Biophysical Society, Rockville, MD, 2002.
50. Becker, W., in *The bh TCSPC Handbook* 2012, Becker & Hickl GmbH
51. Vishwasrao, H.D., et al., *Conformational dependence of intracellular NADH on metabolic state revealed by associated fluorescence anisotropy.* J Biol Chem, 2005. **280**(26): p. 25119-26.
52. Heikal, A.A., S.T. Hess, and W.W. Webb, *Multiphoton molecular spectroscopy and excited-state dynamics of enhanced green fluorescent protein (EGFP): acid–base specificity.* Chemical Physics, 2001. **274**(1): p. 37-55.
53. Zorrilla, S., et al., *Translational and rotational motions of proteins in a protein crowded environment.* Biophysical Chemistry, 2007. **125**(2–3): p. 298-305.
54. Rigler, R., et al., *Fluorescence correlation spectroscopy with high count rate and low background: analysis of translational diffusion.* European Biophysics Journal, 1993. **22**(3): p. 169-175.

55. Terry, B.R., E.K. Matthews, and J. Haseloff, *Molecular characterisation of recombinant green fluorescent protein by fluorescence correlation microscopy.* Biochem Biophys Res Commun, 1995. **217**(1): p. 21-7.
56. Sherman, E., et al., *Using Fluorescence Correlation Spectroscopy to Study Conformational Changes in Denatured Proteins.* Biophys J, 2008. **94**(12): p. 4819-4827.
57. Eggeling, C., et al., *Photobleaching of Fluorescent Dyes under Conditions Used for Single-Molecule Detection: Evidence of Two-Step Photolysis.* Analytical Chemistry, 1998. **70**(13): p. 2651-2659.
58. Ries, J., et al., *Automated suppression ofsample-related artifacts in FluorescenceCorrelation Spectroscopy.* Opt. Express, 2010. **18**(11): p. 11073-11082.
59. Priev, A., et al., *Glycerol Decreases the Volume and Compressibility of Protein Interior†.* Biochemistry, 1996. **35**(7): p. 2061-2066.
60. Timasheff, S.N., *The control of protein stability and association by weak interactions with water: how do solvents affect these processes?* Annual review of biophysics and biomolecular structure, 1993. **22**: p. 67-97.
61. Busch, N.A., T. Kim, and V.A. Bloomfield, *Tracer Diffusion of Proteins in DNA Solutions. 2. Green Fluorescent Protein in Crowded DNA Solutions.* Macromolecules, 2000. **33**(16): p. 5932-5937.
62. Kalwarczyk, T., et al., *Comparative Analysis of Viscosity of Complex Liquids and Cytoplasm of Mammalian Cells at the Nanoscale.* Nano Letters, 2011. **11**(5): p. 2157-2163.
63. Dayel, M.J., E.F. Hom, and A.S. Verkman, *Diffusion of green fluorescent protein in the aqueous-phase lumen of endoplasmic reticulum.* Biophys J, 1999. **76**(5): p. 2843-51.
64. Harland, C.W., M.J. Bradley, and R. Parthasarathy, *Phospholipid bilayers are viscoelastic.* Proceedings of the National Academy of Sciences, 2010. **107**(45): p. 19146-19150.
65. Wang, Z., et al., *Fluorescence correlation spectroscopy investigation of a GFP mutant-enhanced cyan fluorescent protein and its tubulin fusion in living cells with two-photon excitation.* J Biomed Opt, 2004. **9**(2): p. 395-403.
66. Kuimova, M.K., *Mapping viscosity in cells using molecular rotors.* Physical Chemistry Chemical Physics, 2012. **14**(37): p. 12671-12686.
67. Kuttner, Y.Y., et al., *Separating the Contribution of Translational and Rotational Diffusion to Protein Association.* J Am Chem Soc, 2005. **127**(43): p. 15138-15144.
68. Zorrilla, S., et al., *Protein self-association in crowded protein solutions: a time-resolved fluorescence polarization study.* Protein Sci, 2004. **13**(11): p. 2960-9.
69. Fushimi, K. and A.S. Verkman, *Low viscosity in the aqueous domain of cell cytoplasm measured by picosecond polarization microfluorimetry.* The Journal of cell biology, 1991. **112**(4): p. 719-25.
70. Zorrilla, S., G. Rivas, and M.P. Lillo, *Fluorescence anisotropy as a probe to study tracer proteins in crowded solutions.* J Mol Recognit, 2004. **17**(5): p. 408-16.

71. Suhling, K., D.M. Davis, and D. Phillips, *The influence of solvent viscosity on the fluorescence decay and time-resolved anisotropy of green fluorescent protein.* Journal of Fluorescence, 2002. **12**(1): p. 91-95.
72. Strickler, S.J. and R.A. Berg, *Relationship between Absorption Intensity and Fluorescence Lifetime of Molecules.* The Journal of Chemical Physics, 1962. **37**(4): p. 814-822.
73. Peterman, E.J., F. Gittes, and C.F. Schmidt, *Laser-induced heating in optical traps.* Biophys J, 2003. **84**(2): p. 1308-1316.
74. Segur, J.B. and H.E. Oberstar, *Viscosity of Glycerol and Its Aqueous Solutions.* Industrial & Engineering Chemistry, 1951. **43**(9): p. 2117-2120.
75. Nägele, G., *On the dynamics and structure of charge-stabilized suspensions.* Physics Reports, 1996. **272**(5–6): p. 215-372.
76. Bancaud, A., et al., *Molecular crowding affects diffusion and binding of nuclear proteins in heterochromatin and reveals the fractal organization of chromatin.* EMBO J, 2009. **28**(24): p. 3785-98.
77. Minton, A.P., *Confinement as a determinant of macromolecular structure and reactivity.* Biophys J, 1992. **63**(4): p. 1090-1100.
78. Minton, A.P., *The influence of macromolecular crowding and macromolecular confinement on biochemical reactions in physiological media.* J Biol Chem, 2001. **276**(14): p. 10577-80.
79. Ahmad, B., Y. Chen, and L.J. Lapidus, *Aggregation of α-synuclein is kinetically controlled by intramolecular diffusion.* Proceedings of the National Academy of Sciences, 2012. **109**(7): p. 2336-2341.

Appendix I:
Software development for raw anisotropy data: Reformatting and analysis:

A LabView-based program was developed to minimize the time consumed in reformatting parallel and perpendicular fluorescence decays, synchronizing the zero-time, and normalizing the baseline of the two MCP-PMTs. These time-consuming steps were necessary prior to any time-resolved anisotropy decay calculation and fitting using OriginPro. Below, we describe step-by-step usage of this program with the help of screenshot of each page (or operational function) of the software for clarity.

(1) Importing SDT files and zero-time synchronization:

As shown in Figure 3.3, the raw time-resolved, polarization-analyzed data are imported (as .SDT formatted files) from the SPC-830. The zero-time, which is the peak of the instrument response function of the experimental setup, is identified. This zero-time matches the half-point of the rise time from zero signal to the maximum photon count channel. The estimated zero-time is calculated and subtracted from the time-axis of each parallel (Figure 3.3, left) and perpendicularly (Figure A.1.1, right) polarized fluorescence decays.

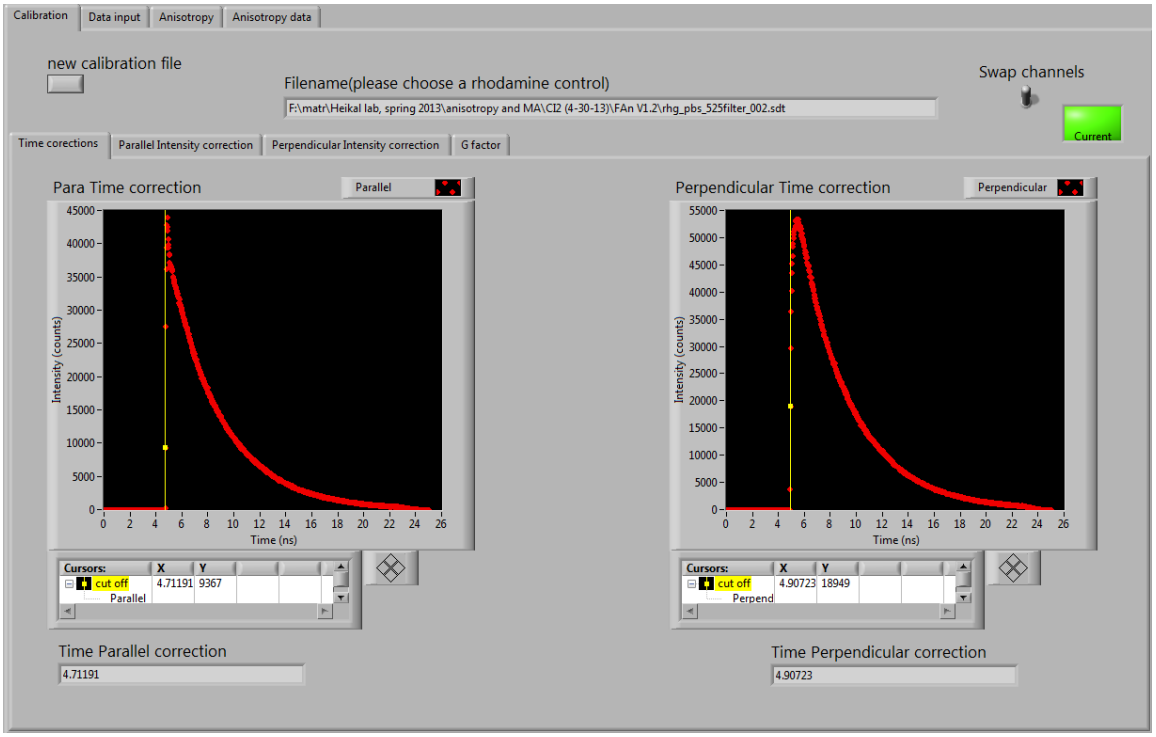

Figure A.1.1 The program adjusts time zero for all of the subsequent files to where the vertical yellow bar is dragged to. This allows both channels to have the same time zero for later work.

(2) Baseline adjustment due to the non-identical MCP-PMTs:

Because the two MCP-PMTs or detection optics are not identical, the baseline of the time-resolved parallel and perpendicularly-polarized fluorescence decays would requires normalization (i.e., to be equated) first (Figure 3.4). The baseline region is first selected to avoid both the non-linear region of the histogram (<1.05 ns region) and the real signal near the zero-time (>3.32 ns) as shown in Figure A.1.2 (right).

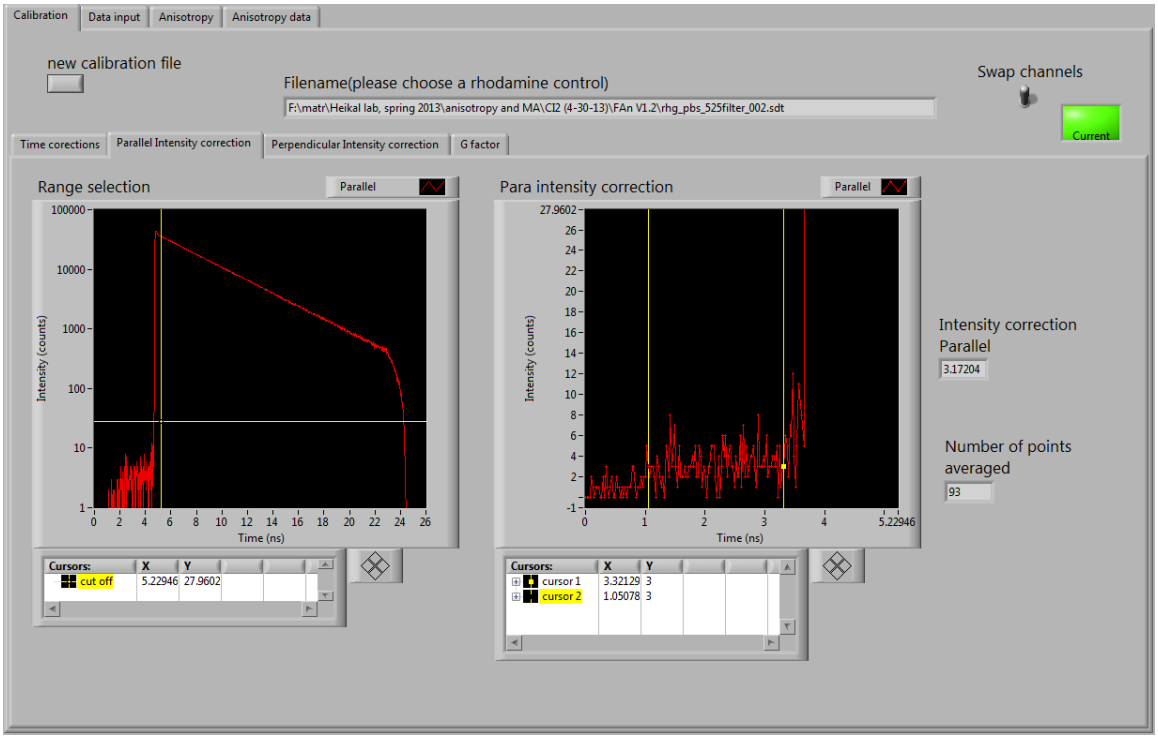

Figure A.1.2 By moving the cursor on the Range selection plot the user can decide what area to focus on in the Intensity correction plot. Then all of the intensity values for data points between the two vertical bars are averaged to determine and then eliminate the background signal noise from subsequent data.

(3) G-factor calculations:

The program is then used to estimate the G-factor using the polarization analyzed decays and tail-matching approach (Figure 3.5). In tail-matching approach [39], a small fluorophore such as fluorescein or rhodamine green is used due to its fast rotational time (~120 ps in water at room temperature) and long fluorescence lifetime (~3.9 ns). Since most of the rotational motion take place during the first couple of hundreds picoseconds, the tails of the fluorescence decays must be equal if the two detectors are not sensitive to polarization. Otherwise, the ratio of the perpendicular-to-parallel fluorescence-tails ratio (Figure A.1.3) is equal to the G-factor that account for polarization-biased detection of the two MCP-PMTs.

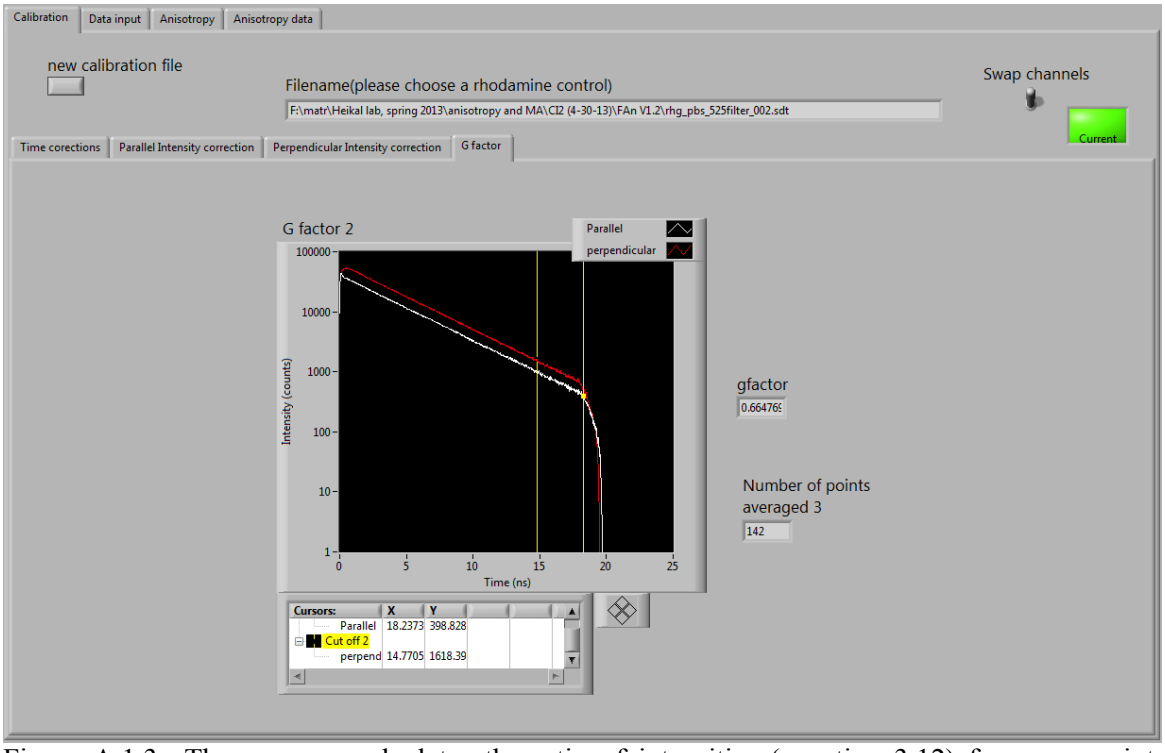

Figure A.1.3 The program calculates the ratio of intensities (equation 3.12) for every point between both vertical bars and then determines the average which is the G-factor.

(4) Data output of the adjusted parallel and perpendicular fluorescence decays:
Once the baseline and zero-time of both parallel and perpendicular fluorescence decays are adjusted, the corresponding two new decays are then created (Figure A.1.4) and ready for time-resolved anisotropy file to be calculated using the estimated G-factor.

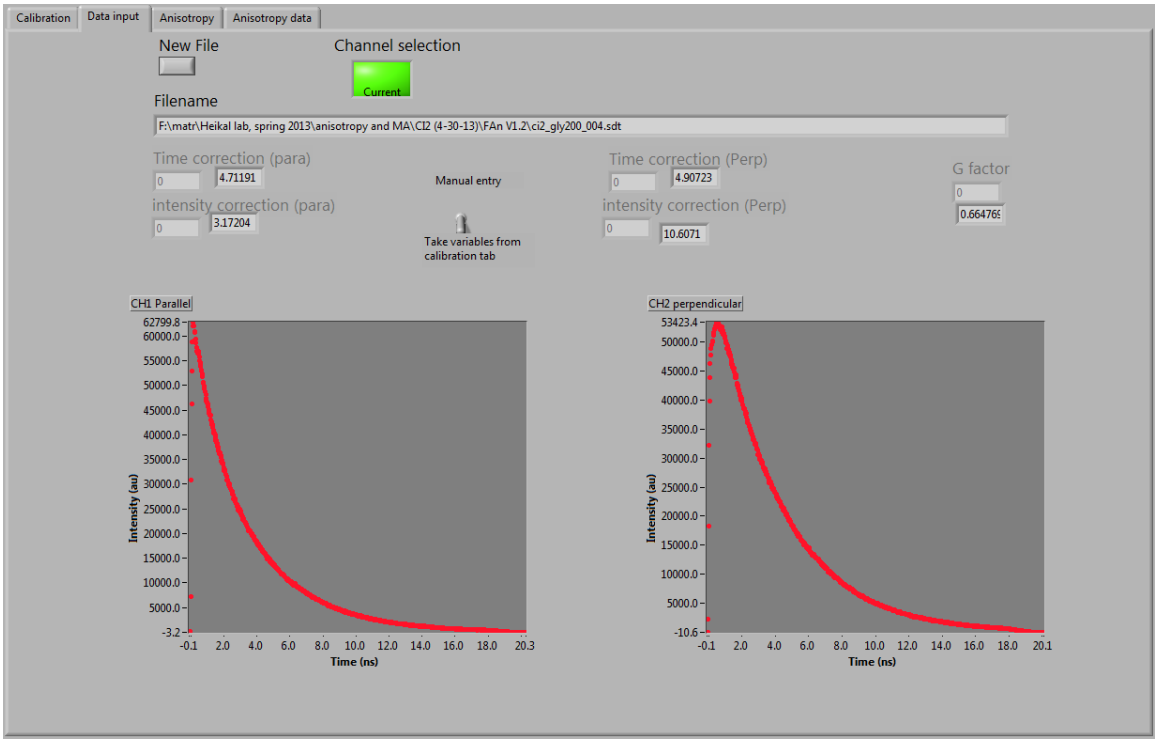

Figure A.1.4 This tab allows the user to select an experimental data .sdt file. It allows for correction values to be manually changed and shows the fluorescence intensity decays for both channels after corrections have been applied.

(5) Anisotropy decay calculations:

The final step is to remove the nonlinear region of the SPC histogram (e.g., >17.5 ns, Figure A.1.5, left). With the estimated G-factor (above), the anisotropy decay is then calculated (Figure A.1.5, right) using the adjusted parallel and perpendicular polarization decays (above). If the G-factor estimation, using the reference fluorophore, is correct, the baseline of the anisotropy decay should be zero following the completion of the corresponding rotational motion (e.g., >12 ns, Figure A.1.5, right).

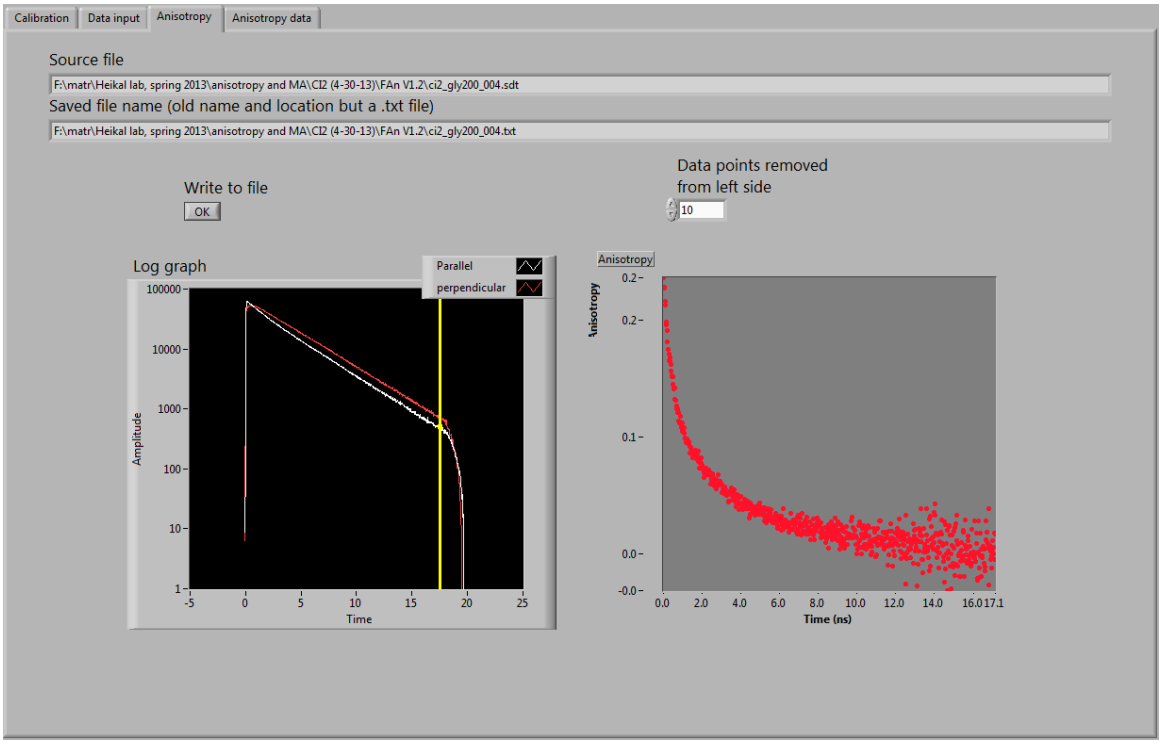

Figure A.1.5the anisotropy tab. The user can remove the tails of the anisotropy decay (noise) and save the decay data as a .txt.

The calculated anisotropy decay (Figure 3.6, right) using this program is then formatted (.txt) and exported to OriginPro for non-linear least-square fitting to calculate the rotational time and the underlying mechanism for rotational diffusion mechanism.

Appendix II:

Microviscosity *versus* bulk viscosity: Crowding, continuum, and technique-specificity

Viscosity, much like temperature, is a property of ensembles of molecules. If temperature is merely the mean kinetic energy of such an ensemble, than viscosity is simply the mean friction that impedes the motion of particles in that ensemble. Considering that mean values depend on the breadth of measurements, it is very easily conceivable that macroscopic measurements of viscosity cannot adequately define viscosity on a microscopic scale. It is with this in mind that this section shall focus on how viscosity can be defined depending on method of observation and the identity of what is observed.

Our experimental work compares viscosity in three different regimes. The first method, using Cannon-Ubbelohde viscometers, are a quintessential bulk measurement. FCS, on the other hand, detects activity in nanoscopic volumes and the short amount of time that it takes to diffuse through that volume. In FAn the diffusing molecule just samples the immediate area in contact with its hydrodynamic volume, on timescales no longer than its fluorescence lifetime.

Method	Volume detected	Time (s)
Ubbelohde Viscometer	15mL	50s-1000s
FCS	<1fL	10us-10ms
Fluorescence anisotropy	Volume of a single fluorescent molecule	Ps-ns

Table A.2.1: Comparison of volumes and timescales of different techniques.

Considering that different intermolecular events (such as collisions) vary depending on the time scale observed microviscosity can be, in part, defined by that time scale. Different regimes of movement occur at different time scales [75], on the shortest timescale ballistic diffusion occurs, as the time scale extends solutes exhibit diffusive behavior. Depending on the solutes/solvent in question solute-solute interactions and structural relaxation will take place on yet other time scales as well [27]. With that in mind, microviscosity measurements might be used as a yardstick for determining the presence of different intermolecular interactions.

The relationship between the size of solvent, or crowding agents, and diffusing species effects how viscosity is interpreted. Generally, the larger the crowding agent is relative to a diffusing species well cause a decrease in the microviscosity observed for the diffusing species. In our FCS experiments with Ficoll 400 the microviscosity affecting the diffusing species increased in relation to tracer size. Other groups have had similar results with various protein probes in variable size dextran solutions [35].

The chemical structure of the crowding agents also appears to affect microviscosity measurements. Protein-protein interactions can decrease the rate of diffusion more so

than would be predicted from bulk viscosity. This is thought to occur from charged and polar residues of different the crowding and diffusing proteins interacting with each other [6]. These interactions increase the friction the diffusing species are affected by, which results in a decrease in diffusion rate.

By comparing different techniques it will be possible to get a clearer picture of cellular environments. By watching the effects of probe size and chemical structure effects diffusion in cellular compartments [76], it should be possible to gain insights in to cytoskeletal organization [77] and other structural components. Aside from just structural information comparing the diffusion of probes with different chemical structures can relate information about the surface properties of the molecules they are interacting with [78]. The dependence of microviscosity on surface (e.g. electrostatic, hydrophobic) interactions [6] could be used to help profile different biological environments. Conversely, structural information pertaining to the native state of proteins as a function of viscosity has been seen [79].

Appendix III:

Growth, purification & fluorescent labeling of CI2

Below is the protocol for preparing CI2 for fluorescence measurements. This protocol has not been fully optimized, but considering the small amount of CI2 needed for FCS and FAn it is has proven more than sufficient. Before attempting to follow this procedure please make sure of the following:

- Make sure that you read all of the instructions and have all of the reagents before starting. Many parts of this protocol require advanced preparation.
- All broths and buffers should be autoclaved before use.
- The growth, lysis, and purification steps ideally take place on the same day to cut down on any potential loss of protein. This takes over 15 hours so I highly recommend having more than one person do it in shifts (with one person doing the growth and the other lysis and purification).
- Make sure that the columns are cleaned and equilibrated before use.
- FCS curves of CI2 in PBS should be very neat, and accurately fit with equation 3.2. If this is not the case, try removing any excess alexaflour.

Growth

1. Make 100 ml of LB broth (directions on side of container) add kanamycin to a final concentration of 50 μg/ml. This is the starter culture.
2. Locate the glycerol stock of *E. coli* with the CI2 plasmid in the -80° freezer. Use a sterile loop to inoculate the starter culture with the glycerol stock, and then immediately put it back in the -80° freezer. (This is a very common procedure. If needed, a more complete explanation is available in the book <u>At the Bench</u> which the lab has a copy of.)
3. Incubate the starter culture overnight, I recommend 12 or more hours, at 37° degrees and 200 RPM, in an orbital shaker.
4. Prepare 900 mL of LB broth with 50 μg/mL kanamycin, preferably on the same day as the starter culture. This is the primary culture.

5. The next morning check and record the OD_{600} of the starter culture on an available nanodrop/uv-vis spec.
6. Pour the starter culture in to the primary culture, and proceed to incubate the primary culture.
7. After a couple of hours start checking the OD_{600} of the primary culture about every 30 minutes. When the absorbance is the same (or within 10%) of the absorbance determined in step 5 the primary culture has entered late log phase and is ready to be induced. This usually takes around 5 hours from inoculation.
8. Induce the primary culture with isopropyl thiogalactopyranoside, IPTG, to a final concentration of 1mM IPTG.
9. Wait 5 hours from inducement and then lyse the E. coli.

Lysis

1. Centrifuge the primary culture at 7,300xg for 20 minutes. If the supernatant is still turbid after centrifugation do it again. When the supernatant is no longer turbid discard it.
2. Resuspend the pellet in 25-40 ml of 50mM Tris (pH 8)
3. Sonicate the suspension on ice. I have been using a Fisher Sonic Dismembrator at 50% power and a 10s on 5s off cycle for 10 minutes. Depending on the sonicator used these settings may be different. Look for manufacturer recommended settings for the probe/sonicator and make sure that the *E. coli* suspension doesn't start bubbling (which is caused by protein denaturation).
4. Centrifuge the solution at 21,000 xg for 30 minutes save supernatant and discard the pellet.
5. Stir the supernatant on ice and add 10% polyethylenimine, PEI, for a total concentration of 0.02%. Let stir for 30 minutes. PEI reacts with air so our current PEI is under N_2.
6. Centrifuge the solution at 21,000 xg for 30 minutes save supernatant and discard the pellet. If the solution is turbid centrifuge again.
7. Sterile filter (0.2 μm filter) the supernatant

8. (optional) place in 4° C refrigerator overnight instead of going right to purification.

Purification

If the Q sepherose column has been taken down then you'll need to follow the following procedure to repack it.

Q Sepherose Column Packing Procedure (adapted from Q Sepharose™ High Performance instructions)

Before starting please locate isopropyl alcohol, and ethanol. Also locate the 1.5x30cm column, peristaltic pump, pump tubing, and appropriate fittings.

1. Suspend 22.1ml Q sepherose gel into a graduated beaker.
2. Rinse with 5-10 gel volumes of nanopure H_2O.
3. Add nanopure H_2O until total volume is 475ml.
4. Rinse column with nanopure H_2O.
5. Wet the bottom filter by injecting 20% ethanol through the effluent tubing.
6. Mount the column vertically on a laboratory stand. Rinse them with nanopure H_2O.
7. Apply nanopure H_2O 2 cm over the column end piece and close the stopcock to the effluent tubing.
8. Pour all the separation media slurry into the column and top up carefully with distilled water.
9. Let the gel bed sediment without using the pump. It takes around 90 minutes.
10. When the level of the bed is stable, close the column outlet. Carefully fill the rest of the column with distilled water to form an upward meniscus at the top and insert the flow adapter. The adapter should be adjusted down to the bed surface.
11. Connect the flow adapter to the pump and open the column outlet.
12. Pump 15% isopropanol through the column for 1 hour at maximum flow (3.1 mm

PVC tubing)**.**

13. Equilibrate with desired buffer (25mM pH8.0 Tris)

Running the column

Note: The column should be equilibrated with 25mM pH8.0 Tris buffer (the same, and only, buffer needed with this part of the procedure) It is important to make sure that the column never runs dry, thankfully q sepherose is not destroyed when it runs dry but it will need to be re-packed with a few column volumes of buffer. Make sure to remove all of the bound protein from the column by running 50 ml of 0.5M NaCl 25mM tris at pH after the column has been used. For more column maintenance information please see the manual for q sepherose (on the GE healthcare web site).

1. Drain the column until the buffer reaches the surface of the matrix bed and close column outlet. To do this in a timely manner it may be necessary to attach a peristaltic pump and run it without buffer.

2. With a transfer pipet, apply the sample gently to the side of the column above bed surface.

3. Open the column outlet until the sample has entered the matrix then reclose the column outlet (use the pump if needed).

4. Gently apply buffer (25mM pH 8.0 Tris) to the side of the column above the bed surface. It is important that the all sample enters the gel at roughly the same time or the protein will elute very broadly. So don't add much buffer in this step.

5. Open the column outlet so the buffer enters the matrix (Carrying with it any remaining sample solution), then close the outlet when the liquid reaches the bed surface.

6. Again add buffer gently to the bed surface, so that when buffer is added in step 8 it doesn't disturb the gel.

7. Hook up the buffer reservoir (the reservoir is just a peristaltic pump which draws

buffer from a bottle). It takes less than 50 ml of buffer to get all of the protein to elute so just use a total of 50ml

8. Proceed to run the 50 ml of buffer through the column. Collect fractions with a fraction collector (fraction size can range from 25 to 50 drops).

9. Measure the OD_{280} of the fractions on a nanodrop/uv-vis spec. CI2 should be in some continuous fractions that have some absorbance, the non CI2 samples should not absorb. The number of fractions depends on the fraction size and how well the sample was added to the column.

10. Discard the non-absorbing fractions. (optional) save the fractions that had a noticeable absorbance at 280nm overnight in a 4° C refrigerator.

11. Combine the fractions and concentrate them with a 3,000MW cutoff Ultra-15 Centrifugal Filter amicon (Millipore). Centrifuge the amicon at 3,000xg in a swinging bucket centrifuge for 30 minutes at 25° C.

12. Determine the concentration of CI2 (extinction coefficient of $7.04 \times 10^3 M^{-1} cm^{-1}$).

13. Save sample in a 4° C refrigerator.

SDS-PAGE

To ensure that only CI2 is present in the eluent I have been running a non-reducing 18% SDS page. In retrospect, it would probably be better to run a reducing SDS-PAGE because the bands have been rather broad and hard to make out. Never the less, this type of SDS-PAGE was able to show a single band of protein in the approximate range of 7kDa. The gel isn't necessary for confirming the identity of CI2 as much as for confirming that there are no other proteins present in the sample.

I have been using the Sheets' group protocol, reagents, and equipment. It is recommended that you consult with the owner of the reagents, and equipment (or the manual) about how to proceed. I will not include a step by step procedure but I will give some advice. I have had the best luck with running the an 18% gel with a 5% loading gel

in a cold room at a 120V, and I have been staining the gel with Coomassie blue and fixing the gel with 40% methanol and 10% acetic acid solution for 30 minutes before rinsing it as well.

Fluorescent Labeling

1. Dissolve alexafluor488 c-5 maleimide (Invitrogen) in DMSO to a concentration of 1-10 mM (ABS 493nm EC: 72000)

2. Replace the buffer that the CI2 is in with 20mM pH7 PBS with an amicon and determine the concentration of the CI2 solution. You will probably need to make dilutions of CI2 to get an accurate measurement.

3. Add the AlexaFluor 488 solution to an aliquot of CI2, so that the dye:protein have a 2:1 molar ratio.

4. Let sit at 25degrees for 4 hours in the dark.

5. Remove unreacted dye by repeated concentration/dilution with 5mM Tris (pH 8) with Amicon Ultra-15 Centrifugal Filter Units (millipore) until flow throw no longer has absorbance at 488 is same as blank.

6. Put the now labeled CI2 in the fridge and confirm that it is CI2 with FCS.

Appendix IV:

Preparation of *E. coli* Lysate.

Below is the protocol for preparing *E. coli* lysate for use as a crowding agent. I have never successfully made or used the lysate but this procedure represents the closest I have come. I think that in this current form the procedure should work (perhaps with minor modification) but the breaking of the lyophilizer I was using prevented me from working on it further.

Growth

1. Make 100 ml of LB broth (directions on side of container) add kanamycin to a final concentration of 50 μg/mL. This is the starter culture.
2. Locate the glycerol stock of *E. coli* with kanamycin resistance in the -80° freezer. Use a sterile loop to inoculate the starter culture with the glycerol stock, and then immediately put it back in the -80° freezer
3. Incubate the starter culture overnight, I recommend 12 or more hours, at 37° degrees and 200 RPM, in an orbital shaker.
4. Prepare 900 mL of LB broth with 50 μg/mL kanamycin, preferably on the same day as the starter culture. This is the primary culture.
5. The next morning check and record the OD_{600} of the starter culture on an available nanodrop/uv-vis spec.
6. Pour the starter culture in to the primary culture, and proceed to incubate the primary culture.
7. After a couple of hours start checking the OD_{600} of the primary culture about every 30 minutes. When the absorbance is the same (or within 10%) of the absorbance determined in step 5 the primary culture has entered late log phase and is ready to be induced. This usually takes around 5 hours from inoculation.

Lysis

1. Centrifuge the primary culture at 7,300xg for 20 minutes. If the supernatant is still turbid after centrifugation do it again. When the supernatant is no longer turbid discard it.
2. Resuspend the pellet in 25-40 ml of 50mM Tris (pH 8)
3. Sonicate the suspension on ice. I have been using a Fisher Sonic Dismembrator at 50% power and a 10s on 5s off cycle for 10 minutes. Depending on the sonicator used these settings may be different. Look for manufacturer recommended settings for the probe/sonicator and make sure that the *E. coli* suspension doesn't start bubbling (which is caused by protein denaturation).
4. Centrifuge the solution at 21,000 xg for 30 minutes save supernatant and discard the pellet.
5. Sterile filter (0.2 μm filter) the supernatant
6. Dialyze against desired buffer (pH 7.6 PBS) overnight at 4° C.

Lyophilize

This section may be problematic considering that the lyophilizer currently in the pharmacy lab is not able to achieve a low enough pressure to properly lyophilize the lysate.

1. Place supernatant in sterile 50 mL centrifuge tubes.
2. Freeze sample
3. Turn on the freeze and pressurize switches on the lyophilizer. And wait until temp is around or below -60° C and the pressure is below 200 mTorr.
4. Make sure the caps are not on the centrifuge tubes and the supernatant is completely frozen.
5. Place the centrifuge tubes in the glass lyophilizer jars.
6. Attach jars to the lyophilizer and **slowly** open the valve that connects the jar to the lyophilizer.
7. Wait until sample is fully lyophilized this may take over 24 hours depending on the amount of fluid being lyophilized.

Lysate crowding agent preparation

1. Re-suspend lyophilized lysate in desired buffer.
2. Determine the concentration of solution with a modified Lowry assay (Thermo scientific)
   The instructions for this assay are kept with the modified Lowry assay kit.